Multiple Lyapunov Function Based Reaching Condition for Orbital Existence of Switching Power Converters

Sudip K. Mazumder, *Senior Member, IEEE*, and Kaustuva Acharya, *Student Member, IEEE*

***Abstract*—A methodology to analyze the reaching condition of a switching power converter (SPC) using Lyapunov's direct method and a piecewise linear model is outlined. By using a multiple Lyapunov function, the reaching criteria for orbital existence of a SPC is formulated as a linear matrix inequality that is solved using a convex optimization solver. Further, the criterion is modified to distinguish the different modes (i.e., sliding and asymptotic modes and combination of the two fundamental modes) of convergences of the reaching dynamics. The applicability of the reaching criteria for solving practical problems using case illustrations of dc–dc converters and three-phase dc–ac converters operating with different control and modulation techniques is demonstrated. The methodology developed in this paper can be potentially extended to other SPCs and may lead to the development of optimal-sequence control techniques that can dynamically change the mode and the rate of convergence of a SPC.**

***Index Terms*—Convergence modes, linear matrix inequality, Lyapunov's stability, piecewise linear (PWL) systems, reaching conditions, switching power converters (SPCs).**

I. Introduction

Conventional stability analyses of switching power converters (SPCs) using averaged models [2], [3] as well as nonlinear maps [4]–[6] assume orbital existence, i.e., that the converters are operating in their steady state. However, for global stability, convergence of the reaching dynamics of an SPC to its orbit needs to be established first. Such analyses can predict whether the state-error trajectories of the SPC converge to its orbit or not for any arbitrary initial condition (either during start-up or transients) and can have a profound impact on the dynamic response of the SPC. In [7]–[14], convergence of the state-error trajectories of a SPC to its orbit has been demonstrated using either time-domain simulations or by numerically solving the differential equations describing the SPC dynamics. However, because these techniques can have significant computational overhead (even for simple SPCs), there exists a need to develop analytical approaches to predict convergence of the SPC state-error trajectories. An analytical approach to predict the reaching condition of a single-switch dc–dc boost SPC has been described in [15]. According to this approach, if the equilibrium solutions of the SPC in the saturated region (i.e., when the switch is permanently turned on or off) are virtual [16] (i.e., not attainable), orbital existence is guaranteed. However, if the equilibrium solutions in the saturated region are real (i.e., attainable), then the orbital existence of the SPC for an arbitrary initial condition depends on the region of attraction of the real solution. The limitations of this approach include the lack of a systematic methodology to determine the saturated *virtual* equilibrium solutions and the region of attractions of the saturated *real* equilibrium solutions, and problems associated with extending the approach to SPCs with multiple switches and higher dimensions, and those operating with time-delayed feedback.

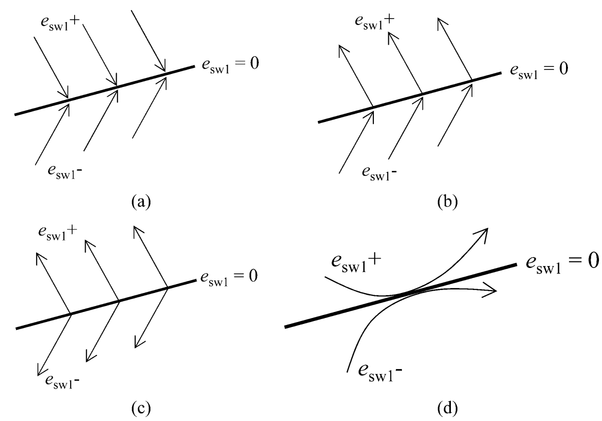

Fig. 1. Schematic illustrating the possible switching-error trajectories for a SPC in the *vicinity* of a switching surface. (a) Trajectories approach the switching surface from both the sides. (b) Trajectories approach the switching surface from one side and leave from the other. (c) Trajectories leave the switching surface from both sides. (d) Trajectories are tangential to the switching surface on either side.

In [17]–[19], a sliding-mode theory based approach has been described, which can be used to determine the existence of the switching surface(s) of a SPC. For a SPC with n switching surfaces, this theory, using a set of common Lyapunov functions, predicts conditions for which the state-error trajectories reach the switching surfaces and once there, slide on these surfaces (i.e., that they satisfy existence) [20]. However, determining the common Lyapunov functions is a key challenge. Furthermore, nonexistence of a common Lyapunov function for a SPC switching model does not preclude orbital existence [24]. Thus,

Manuscript received February 21, 2007; revised December 29, 2007. This work is supported in part by the National Science Foundation (NSF) CAREER Award 0239131 and in part by a Office of Naval Research (ONR) Young Investigator Award N000140510594. Any opinions, findings, conclusions, or recommendations expressed herein are those of the authors and do not necessarily reflect the views of NSF and ONR. Recommended for publication by Associate Editor D. Maksimovic.

S. K. Mazumder is with the Laboratory for Energy and Switching-Electronics Systems, University of Illinoi, Chicago, IL 60607 USA (e-mail: mazumder@ece.uic.edu).

K. Acharya is with the Department of Electrical and Computer Engineering, University of Illinois, Chicago, IL 60607 USA.

Color versions of one or more of the figures in this paper are available online at http://ieeexplore.ieee.org.

Digital Object Identifier 10.1109/TPEL.2008.921065

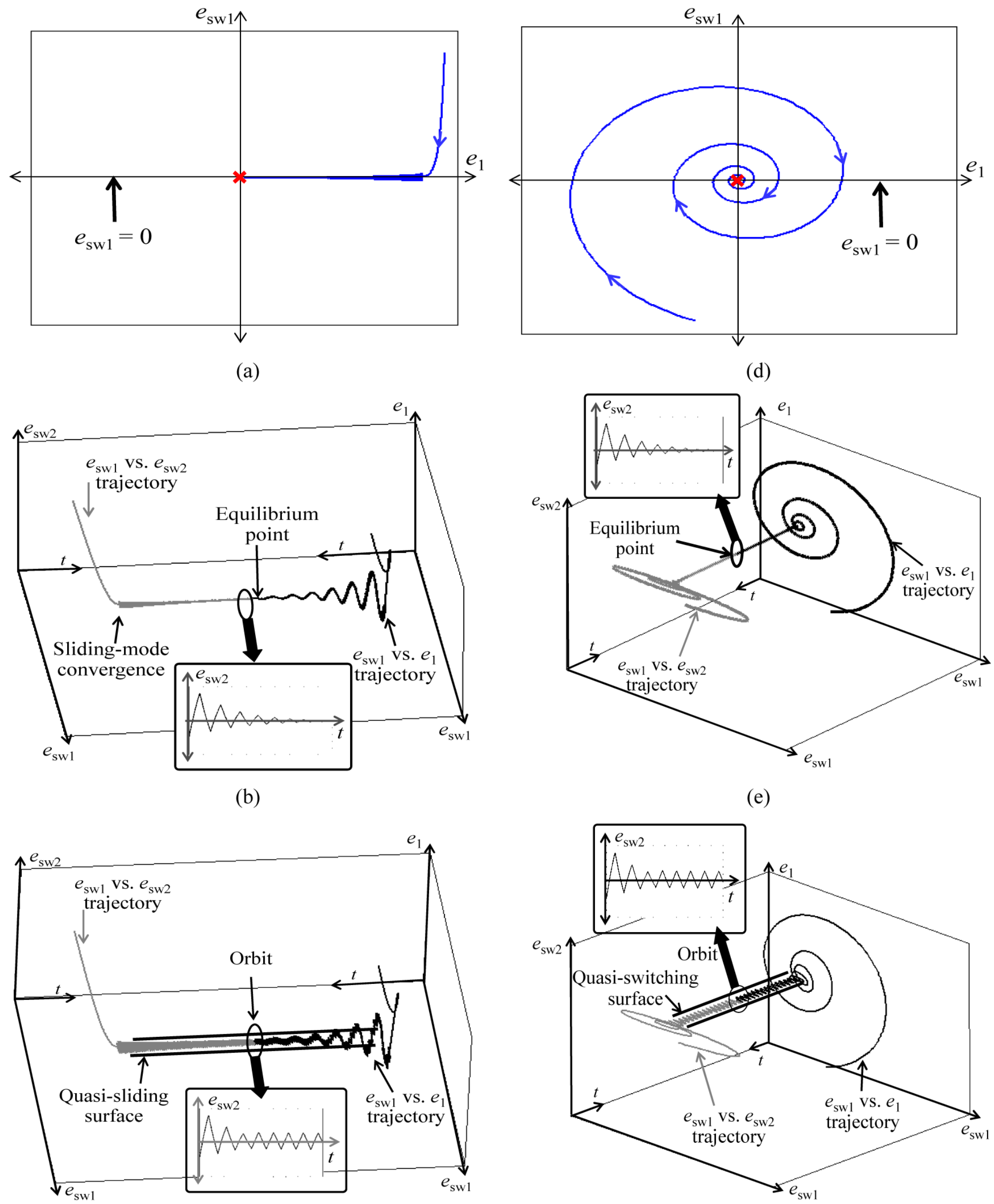

Fig. 2. Schematics illustrating (a)–(c) sliding and (d)–(f) asymptotic modes of convergences for a SPC. (a) and (d) Convergence modes for a SPC with a single ideal switching surface. (b) and (e) Convergence dynamics for a SPC with two ideal switching surfaces. (c) and (f) Convergence dynamics for a SPC with two quasi-ideal switching surfaces.

sliding-mode theory only predicts sliding-mode convergence but, not asymptotic or mixed-mode (combination of the sliding and asymptotic modes) convergences.

Because of the above-mentioned limitations, there exists a need to develop new analytical criteria for orbital existence of SPC switching models. Since the dynamics of a SPC can be captured using a piecewise linear (PWL) model [1], recent works in the hybrid systems and controls community (as outlined in [21] and references therein) are of relevance. For instance, in [21], the author proposes a technique for PWL system based on multiple Lyapunov functions to predict the dynamics and convergence of the states to the equilibrium. However, unlike a SPC (where the steady-state exhibits orbital motion), for the PWL systems considered in [21], the equilibrium is a fixed point. This is because, in a practical SPC, the switching surfaces are not ideal and there exists a finite boundary layer around each switching surface. As described in Sections III and IV, this complicates the analysis of orbital existence of a multi-switch SPC. For instance, in a parallel SPC, if one or more converter operates with more than one switching state in a finite time interval while the rest of the converters do not change states, the relative duration of the sequences over the time interval needs to be considered for orbital existence. Finally, the techniques in [21] also have to be modified for time-delayed PWL systems (such as networked SPCs [23]).

Therefore, in this paper, we modify the multiple Lyapunov function based criterion in [21] to predict the reaching criterion for orbital existence of SPCs. First, in Section II, the various reaching mechanisms of a SPC with ideal and quasi-ideal switching surfaces [20] are illustrated. For both of these cases, the reaching dynamics of the SPC under asymptotic as well as sliding-mode conditions are illustrated. Subsequently, in Section III, we describe a PWL model of the SPC. Such a model can describe the dynamics of several dc–dc as well as multiphase dc–ac/ac–dc/ac–ac SPCs (modeled in synchronous reference frame). Subsequently, we derive the reaching criterion for orbital existence and also demonstrate how the criterion can be modified to distinguish among the different convergence modes. The multiple Lyapunov functions are determined by formulating a convex optimization problems using the PWL model of a SPC (that operate with or without feedback delay) and solving the resulting linear-matrix inequality (LMI) [22] using a standard LMI solver.

Finally, in Section IV, the application of the reaching criteria for different SPCs is illustrated. The reaching criteria can be used to supplement existing steady-state stability analyses techniques (either based on small-signal averaged models [2], [3] or nonlinear techniques using maps [4]–[6]) to predict the global stability of SPCs. Further, the knowledge of the modes of convergence of the reaching dynamics (asymptotic-, sliding-mode-, or mixed-mode-convergences) can potentially facilitate design of SPCs with faster dynamics responses. To demonstrate the wide application of the reaching criteria proposed in this paper, the following practical case illustrations are demonstrated.

- Single-switch dc–dc boost SPC: For this SPC, the impacts of parameter variations, control schemes and modulation strategies on the reaching conditions are investigated. Further, a comparison of the reaching conditions of the SPC operating in continuous conduction mode (CCM) and discontinuous conduction mode (DCM) is presented.
- Multimodule parallel dc–dc boost SPC: For this SPC, a comparison of the impacts of synchronous modulation and interleaved modulation on the reaching conditions is presented.
- Cascaded SPC comprising a single-switch dc–dc boost SPC followed by a single-switch dc–dc buck SPC: For this SPC, the impacts of different start-up mechanisms on the reaching conditions are investigated.
- Network of parallel-connected three-phase voltage-source inverters (VSIs): For such SPCs, control information is exchanged over a communication network [23]. The impacts of the time delay (which is inherent in such information exchange) on the reaching condition are investigated.

II. Illustrations of Reaching Mechanisms for SPCs With Ideal and Quasi-Ideal Switching Surfaces

Due to the switching actions of the power devices, the dynamical model of a typical SPC is discontinuous in nature [20]. The solution of such models is defined everywhere except at the surfaces of discontinuities (i.e., at the switching surfaces). Fig. 1 illustrates all (theoretically) possible switching-error trajectories $(e_{\rm sw1})$ for a SPC in the vicinity of an "ideal" discontinuous surface $(e_{\rm sw1} = 0)$. The power devices of the SPC are turned on or off depending on whether the switching-error trajectory lies above or below the switching surface $e_{\rm sw1} = 0$. Of these,

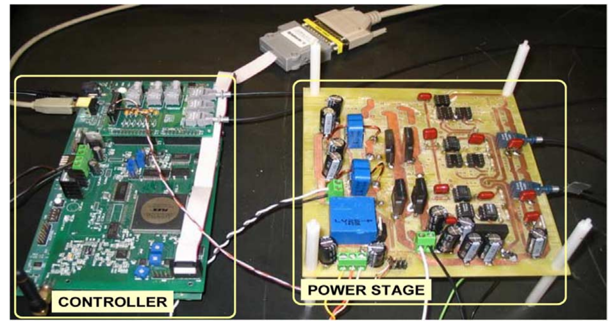

Fig. 3. Experimental setup of a dc–dc SPC with two modules. The board is designed to perform experiments on single-module dc–dc boost SPC (Fig. 4), two-module parallel dc–dc boost SPC (Fig. 10), and a cascaded SPC consisting of a front end boost SPC followed by a buck SPC (Fig. 14).

trajectories illustrated in Fig. 1(c) are not physically stabilizable (because the trajectories leave the switching surface from either side), while dynamics in Fig. 1(d) are inadmissible for SPCs (because the trajectories move tangentially to the switching surface) and hence they cannot lead to switching. Only the trajectories outlined in Fig. 1(a) and (b) are of practical relevance.

Fig. 1(a) illustrates sliding motion [17], [18] because the trajectories on either side of the switching surface point towards it. For a second-order system with one switching surface $e_{\rm sw1} = 0$, such a dynamics is illustrated in Fig. 2(a). The plot between $e_{\rm sw1}$ and e_1 (that represents one of the states of the SPC in error coordinates) shows that once $e_{\rm sw1}$ hits the switching surface, it stays in its neighborhood. The dynamics of the resultant reduced-order model on the sliding manifold is assumed to be smooth and hence, the stability of the motion can be determined by conventional techniques [20]. For a stable system, as $e_1 \rightarrow 0$ on the sliding manifold, switching occurs at progressively faster repetition rates culminating at infinity corresponding to the point $e_1 = e_{\rm sw1} = 0$ [18], [20].

On the same note, Fig. 2(b) illustrates the dynamics of a higher order SPC with two switching surfaces $(e_{\rm sw1} = 0$ and $e_{\rm sw2} = 0)$ and another state in error coordinates (e_1) with varying time (t). This is plotted as two separate trajectories (*because the dimension of the system including time is four*): one illustrating the evolution of $(e_{\rm sw1}$ and $e_{\rm sw2})$ with t, while the second illustrating the mirror image of the evolution of $(e_{\rm sw1}$ and $e_1)$ with t. In the figure, these two trajectories are symmetric (in t) about the equilibrium point. The plot shows that the trajectory described by $(e_{\rm sw1}, e_{\rm sw2},$ and $t)$ exhibits sliding motion and $e_1 \rightarrow 0$ on the sliding manifold. Eventually convergence occurs at $e_1 = e_{\rm sw1} = e_{\rm sw2} = 0$ when the switching frequency is infinite.

In general, for a SPC described by an nth-order dynamical system and comprising m sliding surfaces, the order of the dynamical system on the sliding surface is $n - m$ [17]. If the reduced-order dynamical system is stable, the error trajectories reach the equilibrium point when the switching frequency approaches infinity. On the whole, the reaching dynamics for such a system has to be investigated in two steps: one which predicts reaching up to the sliding manifold and the other, which predicts convergence of the reduced-order motion on the sliding manifold to the equilibrium.

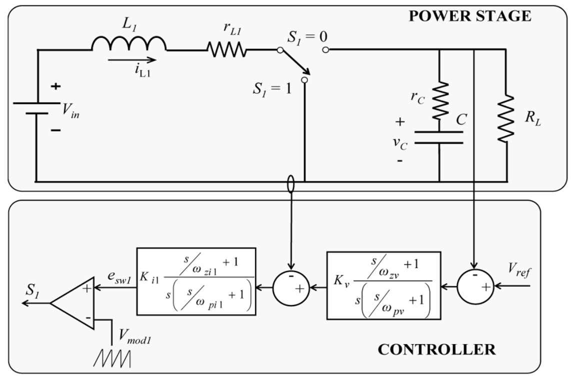

$$\dot{x} = A_{0i}x + B_i$$

$$x = \begin{bmatrix} i_{L1} \\ v_C \\ \xi_1 \\ \xi_2 \\ \xi_3 \\ \xi_4 \end{bmatrix} \qquad A_{0i} = \begin{bmatrix} \multicolumn{2}{c}{A_{p\_i}} & \multicolumn{4}{c}{0_{2\times4}} \\ 0 & -1 & 0 & 0 & 0 & 0 \\ 0 & 0 & K_v & K_v\omega_{zv} & -\omega_{pi1} & 0 \\ -1 & 0 & 0 & 0 & 0 & 0 \\ 0 & 0 & 0 & 0 & 1 & 0 \end{bmatrix} \qquad B_i = \begin{bmatrix} \frac{V_{in}}{L_1} \\ 0 \\ V_{ref} \\ 0 \\ 0 \\ 0 \end{bmatrix}$$

Switching conditions:
$$S_1 = \begin{cases} 0 & \left(K_{i1}\xi_3 + K_{i1}\omega_{zi1}\xi_4\right) - V_{mod\,1} \le 0 \\ 1 & \left(K_{i1}\xi_3 + K_{i1}\omega_{zi1}\xi_4\right) - V_{mod\,1} > 0 \end{cases}.$$

Fig. 4. Schematic and state-space equations of the power stage and current-mode controller of a single-switch dc–dc boost SPC. The matrix A_{p_i} for a single-switch dc–dc boost SPC (along with other single-module SPCs) is given in Appendix A. $0_{p\times q}$ represents a matrix with p rows and q columns, all of whose elements are zero.

TABLE I
PARAMETERS OF THE SINGLE-SWITCH DC–DC BOOST SPC (FIG. 4)

POWER STAGE		CONTROLLER	
Parameter	**Nominal Values**	**Parameter**	**Nominal Values**
Switching frequency	100 kHz	Voltage controller gain, K_v	10000
Output voltage	10 V	Voltage controller zero, ω_{zv}	100 rad/s
Peak output power	20 W	Voltage controller pole, ω_{pv}	20000 rad/s
Input inductance	128 μH	Current controller gain, K_{i1}	15000
Output capacitance	1000 μF	Current controller zero, ω_{zi1}	1000 rad/s
		Current controller pole, ω_{pi1}	25000 rad/s

A practical SPC, however, is not designed to achieve an infinite switching frequency. For such a system, as shown in Fig. 2(c), an ideal sliding manifold is replaced with a quasi-sliding surface (which ensures *finite* switching frequency). For such a case, the equilibrium point is replaced with an orbit, which has infinite possibilities including periodic-, quasi-periodic-, and chaotic-orbits [4]–[6]. Thus, convergence of reaching dynamics of a finite-frequency SPC culminates in an orbit and not an equilibrium point as in the case of ideal sliding motion.

Now, if the trajectories in the vicinity of a switching surface, as illustrated in Fig. 1(b), approach the switching surface from one side and leave it from the other, reaching dynamics of the corresponding SPC, with ideal or quasi-ideal switching surface(s), can converge, respectively, to its equilibrium point or orbit asymptotically. Thus, the SPC reaching dynamics exhibits no sliding motion. By following the same rationale as outlined above for the cases illustrated in Fig. 2(a)–(c), one can explain the reaching dynamics of the SPC for asymptotic convergence [as illustrated in Fig. 2(d)–(f)] for the ideal and quasi-ideal switching surfaces. Once again, for the ideal case, the switching frequency of the SPC on reaching equilibrium is infinity; while for the quasi-ideal case, a finite-frequency orbital motion is attained. However, unlike sliding-mode dynamics, which has two modes of convergences, reaching dynamics for asymptotic convergence has only one mode since all the states converge at the same time to the equilibrium point or the orbit.

Finally, the reaching dynamics of a SPC can also exhibit a combination of sliding- and asymptotic-modes of convergences, which will be referred to as mixed-mode dynamics in this paper. Such dynamics can occur if the parameters or the operating conditions of the SPC undergo a change when the SPC is going through a start-up or transient. If such a change results in a transition of the SPC dynamics from one convergence mode to the other, the overall mode of convergence is referred to as the mixed-mode convergence.

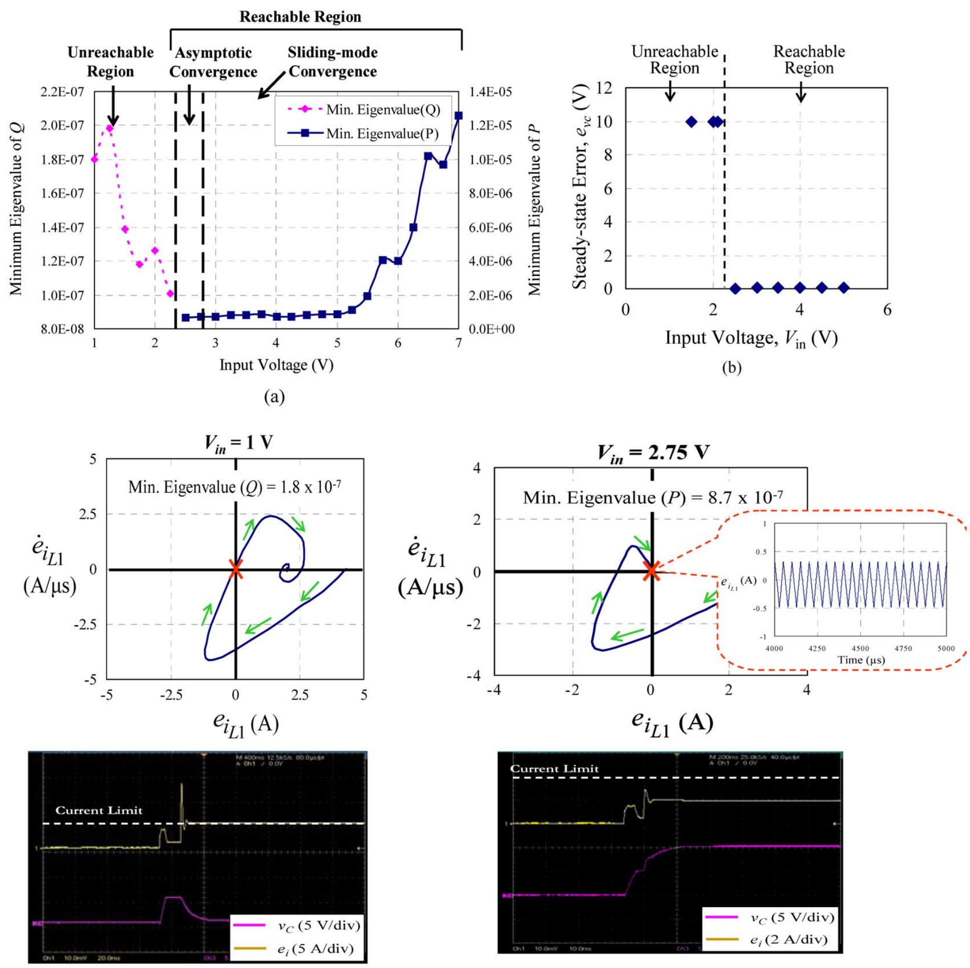

(c)

Fig. 5. (a) Variation of the minimum eigenvalues of the augmented P and Q matrices (obtained by solving LMIs (7), (12), and (10) for asymptotic convergence, sliding-mode convergence, and unreachable regions, respectively) with input voltage for a single-switch dc–dc SPC with current-mode control and operating in CCM. (b) Experimental results illustrating the reachable and unreachable regions with variation of the input voltage, $V_{\rm in}$. (c) Experimental results illustrating state-error trajectories in the reachable ($V_{\rm in} = 2.75$ V) and unreachable ($V_{\rm in} = 1$ V) regions. In (c), the error dynamics in the steady-state is also presented for the reachable case. To obtain the phase portrait for this case and for the subsequent examples, the experimental data (from the oscilloscope) is retrieved as a data file and plotted in the error coordinates.

III. Derivation of Reaching Criteria

The class of SPCs considered in this paper can be described by the following PWL state-space equation:

$$\dot{x}(t) = A_{0i}x(t) + A_{1i}x(t-\tau_d) + B_i. \tag{1a}$$

In (1a), i is an integer that represents the switching state of a SPC, $x(t) \in \Re^n$ represent the SPC states, $A_{0i} \in \Re^{n\times n}$ and $A_{1i} \in \Re^{n\times n}$ are matrices, $B_i \in \Re^n$ is a column vector, and τ_d represents the feedback time delay. Note that the SPC model is nonlinear due to switching among the various PWL models described by (1a). In this paper, only SPCs with linear controllers and loads are considered. For SPCs with nonlinear controllers or loads, the SPC dynamics can be described by piecewise nonlinear models; therefore, the analyses technique has to be modified [24]. From this point onwards, the notation of time is dropped and an arbitrary time-delayed vector $y(t-\varphi)$ is represented as y_φ or $y(t+\varphi)$ as $y_{-\varphi}$. Thus, (1a) can be re-written as

$$\dot{x} = A_{0i}x + A_{1i}x_{\tau_d} + B_i. \tag{1b}$$

Next, (1b) is translated to the error coordinates using $\overline{e} = x^* - x$, where $\overline{e}$ represents the error vector and x^* represents the steady-state values of the SPC states when the switching frequency is infinity. The modified state-space equation is given by

$$\dot{\overline{e}} = A_{0i}\overline{e} + A_{1i}\overline{e}_{\tau_d} - (A_{0i} + A_{1i})x^* - B_i. \tag{2a}$$

Equation (2a) can be rewritten as

$$\dot{\overline{e}} = (A_{0i} + A_{1i})\overline{e} + A_{1i}\left(\overline{e}_{\tau_d} - \overline{e}\right) - (A_{0i} + A_{1i})x^* - B_i. \tag{2b}$$

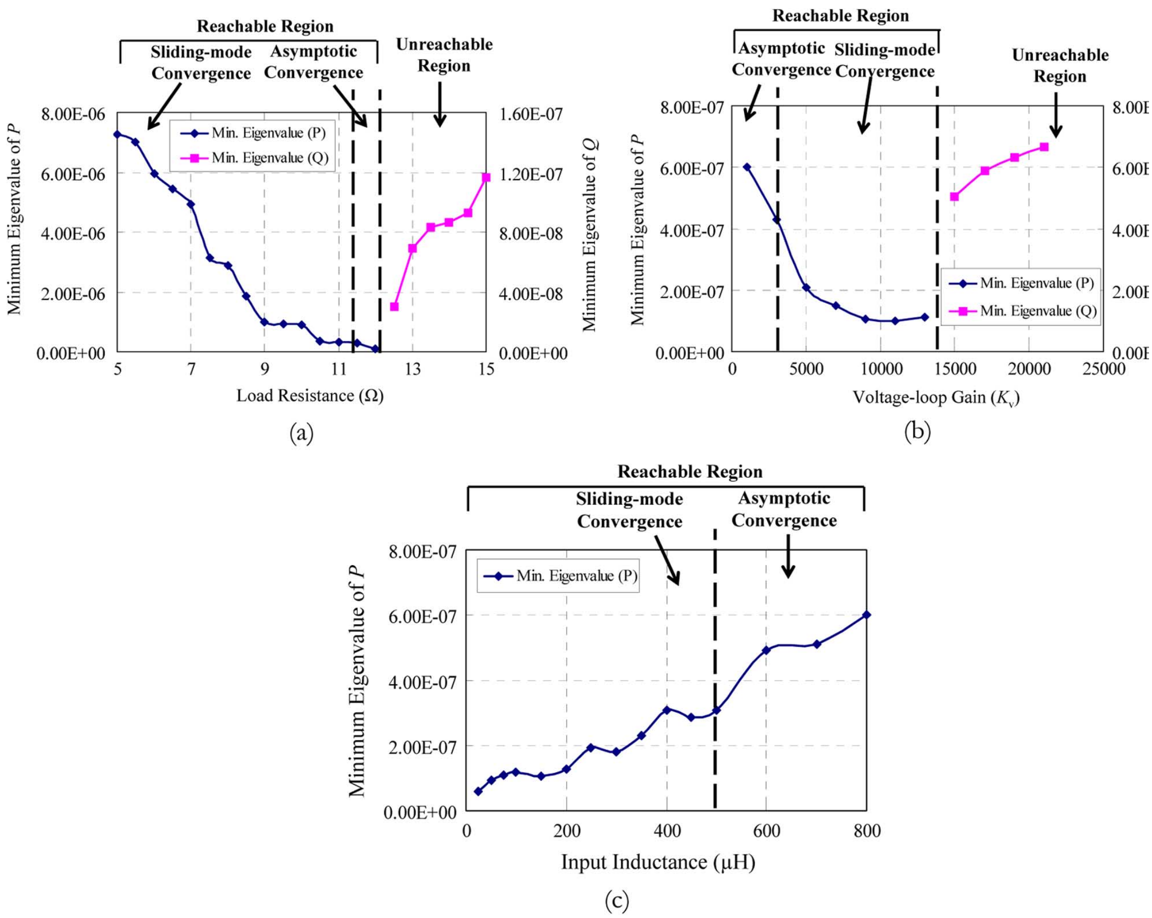

Fig. 6. Variation of the minimum eigenvalues of the augmented P and Q matrices (obtained by solving LMIs (7), (12), and (10) for asymptotic convergence, sliding-mode convergence, and unreachable regions, respectively) with (a) load resistance ($V_{\rm in} = 3.5$ V, $K_{\rm v} = 10000, L_1 = 128\,\mu$H), (b) controller voltage-loop gain ($V_{\rm in} = 3.5$ V, $L_1 = 128\,\mu$H, $R_{\rm L} = 5\ \Omega$), and input inductance ($V_{\rm in} = 3.5$ V, $K_{\rm v} = 10000, R_{\rm L} = 5\ \Omega$).

Using

$$\begin{aligned}\overline{e}_{\tau_d} - \overline{e} &= -[\overline{e}_{-\tau}]_{\tau=-\tau_d}^{\tau=0} \\ &= \int_{-\tau_d}^{0} (-A_{0i}\overline{e}_{-\tau} - A_{1i}\overline{e}_{(\tau_d-\tau)} + (A_{0i}+A_{1i})x^* + B_i)d\tau\end{aligned}$$

delay model (2b) in $\overline{e}$ can be transformed to a distributed form in variable e

$$\dot{e} = (A_{0i}+A_{1i})e - \int_{-\tau_d}^{0} A_{1i}A_{0i}e_{-\tau}d\tau - \int_{-2\tau_d}^{-\tau_d} A_{1i}^2 e_{-\tau}d\tau + \bar{B}_i \tag{2c}$$

where

$$\bar{B}_i = -B_i - (A_{0i}+A_{1i})x^* + \tau_d A_{1i}(B_i + (A_{0i}+A_{1i})x^*)$$

and stability of (2c) implies stability of (2b).

A. Reaching Criteria Development

The *reaching criteria* of a SPC depends on the number of noncomplementary switching functions, and the sequence of switching states, which are generated by the noncomplementary switching functions. To analyze the convergence of SPC state-error trajectories, all possible nonredundant switching states and nonrepetitive switching sequences that are obtained using the noncomplementary switching functions have to be determined. They are defined and illustrated below.

- ***Complementary switching functions***: Complementary switching functions are defined for a set of switches where, if one switch is turned on, the other is turned off and vice versa. For instance, a single-module dc–dc boost SPC with one controllable switch, as shown in Fig. 4, has one noncomplementary switching function. For such a SPC operating in CCM, i can take two values, namely $i = 1$ for $S_1 = 0$ and $i = 2$ for $S_1 = 1$. On the other hand, a single-module dc–dc synchronous SPC with two controllable switches (that operate complementarily) also has one switching function (if dead-times are ignored). However, if the SPC in Fig. 4 operates in DCM, i can take three values, namely $i = 1$ for $S_1 = 0_{\rm C}, i = 2$ for $S_1 = 0_{\rm D}$, and $i = 3$ for $S_1 = 1$, where $0_{\rm C}$ represents the switching state, when the controllable switch is turned off

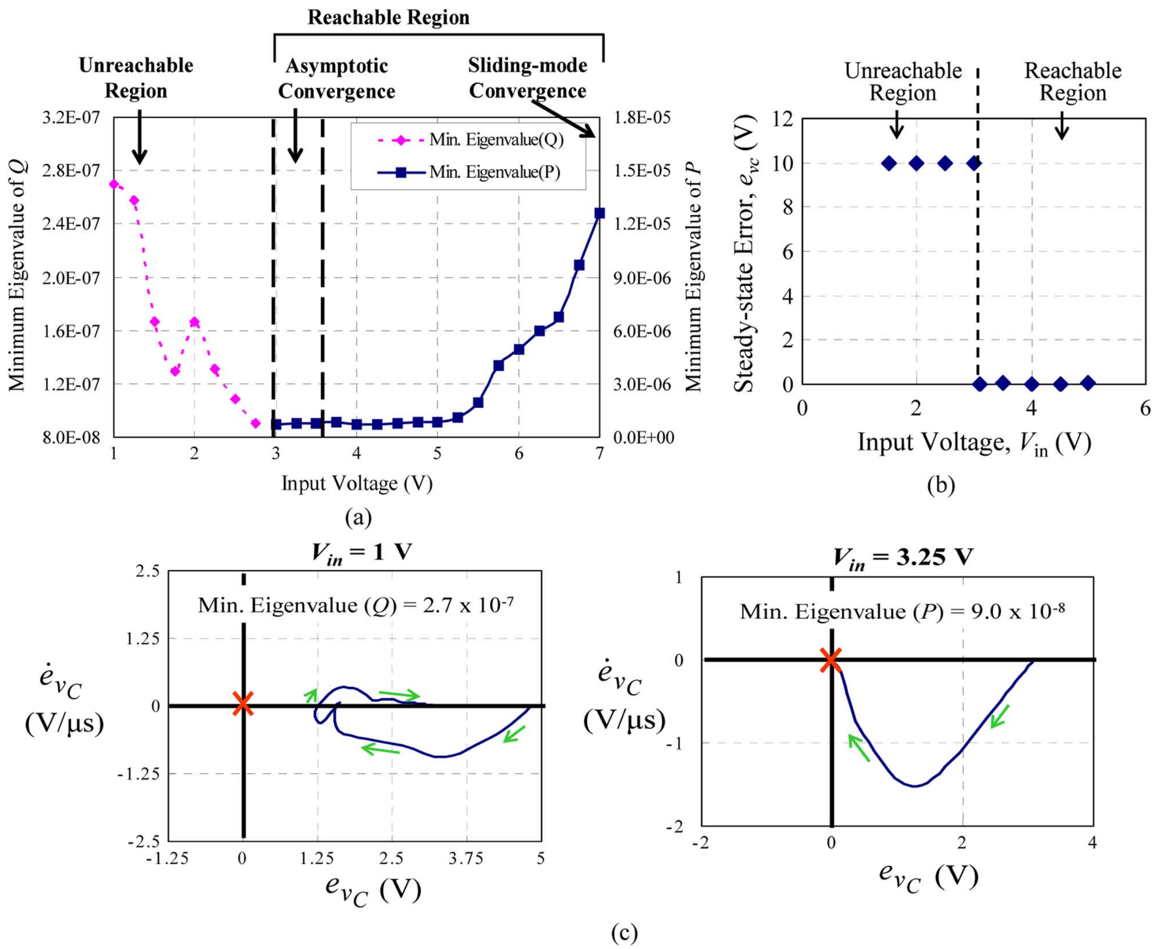

Fig. 7. (a) Variation of the minimum eigenvalues of the augmented P and Q matrices (obtained by solving LMIs (7), (12), and (10) for asymptotic convergence, sliding-mode convergence, and unreachable regions, respectively) with input voltage for a single-switch dc–dc SPC with voltage-mode control and operating in CCM. (b) Experimental results illustrating the reachable and unreachable regions with variation of the input voltage V_{in}. (b) Experimental results illustrating state-error trajectories in the reachable ($V_{\text{in}} = 3.25$ V) and unreachable ($V_{\text{in}} = 1$ V) regions.

and the inductor current of the SPC has a nonzero value, while 0_{D} represent the case, when the controllable switch is turned off and the inductor current is zero.

- ***Redundant switching states***: Two switching states are classified as redundant states, if the state-space equations of the SPC corresponding to those switching states are identical. For instance, for each module of a three-phase voltage-source inverter, as shown in Fig. 17, with three noncomplementary switching functions S_{r1}, S_{r2} and S_{r3}, the switching states $(S_{r1} = 0, S_{r2} = 0, S_{r3} = 0)$, and $(S_{r1} = 1, S_{r2} = 1, S_{r3} = 1)$ are redundant states (where the value of r varies from 1–6) and can be described by the same state-space equation.
- ***Nonrepetitive switching sequences***: Two switching sequences are classified as repetitive sequences, if they consist of the same set of switching states, occurring not necessarily in the same order. For instance, for a single-module dc–dc boost SPC, as shown in Fig. 4, operating in CCM, the sequence of $S_1 = 0$ followed by $S_1 = 1$ (i.e., $0 \to 1$) or $S_1 = 1$ followed by $S_1 = 0$ (i.e., $1 \to 0$) represent repetitive states. From the standpoint of reaching-criteria development, two or more repetitive sequence of states leads to the same conclusion. Hence, only nonrepetitive switching sequences are considered for the reaching condition analyses.

In general, the total number of feasible combinations of nonrepetitive switching sequences for an SPC operating in CCM is given by

$$M = \sum_{l=1}^{(2^N - W)} \left({}^{(2^N - W)}C_l \right) = \sum_{l=1}^{(2^N - W)} \left(\frac{(2^N - W)!}{l!(2^N - W - l)!} \right) \tag{3a}$$

where N is the total number of noncomplementary switching functions and W is the number of redundant switching states. For a SPC (with N noncomplementary switching functions) operating in DCM, the number of feasible nonrepetitive switching sequences is given by

$$M = \sum_{l=1}^{(3^N - W)} \left({}^{(3^N - W)}C_l \right) = \sum_{l=1}^{(3^N - W)} \left(\frac{(3^N - W)!}{l!(3^N - W - l)!} \right). \tag{3b}$$

This is because the number of switching states that each noncomplementary switching function can attain when the SPC is

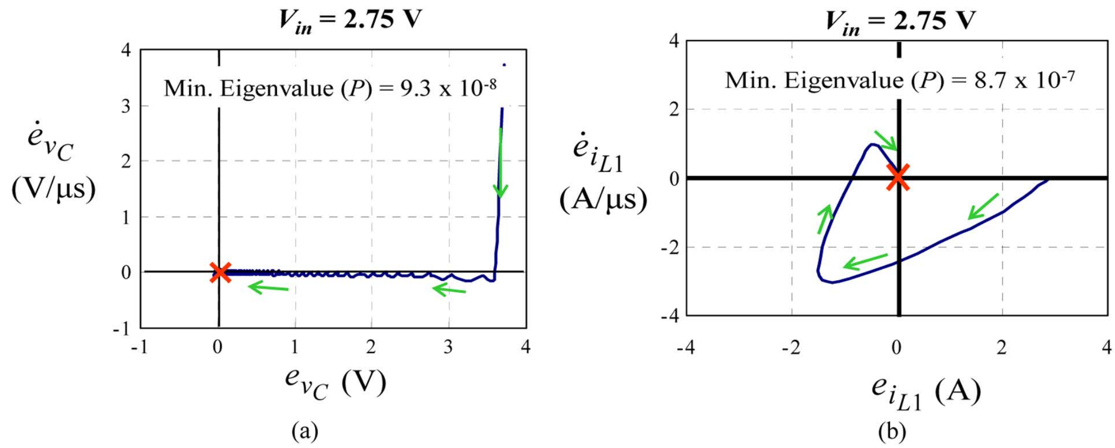

Fig. 8. Experimental results, illustrating state-error trajectories of a single-switch dc–dc boost SPC with (a) hysteretic modulation and (b) carrier-based PWM. The state-error trajectories exhibit sliding and asymptotic modes of convergence for the two cases, respectively.

operating in DCM is three. In Appendix B, the procedure to obtain (3a) and (3b) is illustrated.

To determine the reaching criterion of a SPC, a convex combination of multiple, positive-definite, quadratic Lyapunov function, $V_k(e) > 0$ (for the kth switching sequence) is defined, which is given by [21]

$$V_k(e) = \sum_{i=1}^{h} \alpha_{ki} e^T P_{ki} e, \quad k = 1, 2, \ldots, M \tag{4}$$

where h is the number of switching states in a given sequence, $0 \le \alpha_{ki} \le 1, \sum_{i=1}^{h} \alpha_{ki} = 1, P_{ki} = P_{ki}^T$ is a positive-definite matrix, and $pV_k(e) > V_k(e_{-\tau})$, for any $-2\tau_d \le \tau \le 0$ and $p > 1$. Note that, for a positive-definite matrix, all of its eigenvalues are positive and hence, the minimum eigenvalue of P_{ki} is greater than zero [25]. In Section IV, this property is used to demonstrate the reachability bounds of the SPCs.

According to Lyapunov's criterion, the trajectories of the SPC converge towards the orbit for finite switching frequency (or the equilibrium point for infinite switching frequency) provided $\dot{V}_k(e) < 0$. To evaluate if (2c) satisfies this criterion, we obtain the derivative of $V_k(e)$ in (4), which is given by

$$\dot{V}_k(e) = \sum_{i=1}^{h} \alpha_{ki} (\dot{e}^T P_{ki} e + e^T P_{ki} \dot{e}). \tag{5a}$$

Using (2c), (5a) can be re-written in the matrix format as (5b), shown at the bottom of the page. For any $\gamma > 0$ and because the Lyapunov function (4) satisfies $pV_k(e) > V_k(e_{-\tau})$ (for any $p > 1$), we have $\gamma(pV_k(e) - V_k(e_{-\tau})) > 0$. Therefore, by adding this term to (5b), we obtain the inequality in (5c), shown at the bottom of the page. This inequality can be rearranged in a matrix format as (5d), shown at the bottom of the next page. For constant matrices[1] R_0 and R_1, we can modify the matrix

$$\dot{V}_k(e) = \sum_{i=1}^{h} \alpha_{ki} \left(\begin{array}{l} \begin{bmatrix} e \\ 1 \end{bmatrix}^T \begin{bmatrix} (A_{0i}+A_{1i})^T P_{ki} + P_{ki}(A_{0i}+A_{1i}) & \bar{B}_i^T P_{ki} \\ P_{ki}\bar{B}_i & 0 \end{bmatrix} \begin{bmatrix} e \\ 1 \end{bmatrix} + \\ \int_{-\tau_d}^{0} \left(e_{-\tau}^T (-A_{1i}A_{0i})^T P_{ki} e + e^T P_{ki} (-A_{1i}A_{0i}) e_{-\tau} \right) d\tau + \\ \int_{-2\tau_d}^{-\tau_d} \left(e_{-\tau}^T \left(-A_{1i}^2\right)^T P_{ki} e(t) + e^T(t) P_{ki} \left(-A_{1i}^2\right) e_{-\tau} \right) d\tau \end{array} \right) \tag{5b}$$

$$\dot{V}_k(e) < \sum_{i=1}^{h} \alpha_{ki} \left(\begin{array}{l} \begin{bmatrix} e \\ 1 \end{bmatrix}^T \begin{bmatrix} (A_{0i}+A_{1i})^T P_{ki} + P_{ki}(A_{0i}+A_{1i}) & \bar{B}_i^T P_{ki} \\ P_{ki}\bar{B}_i & 0 \end{bmatrix} \begin{bmatrix} e \\ 1 \end{bmatrix} + \\ \int_{-\tau_d}^{0} \left(e_{-\tau}^T (-A_{1i}A_{0i})^T P_{ki} e + e^T P_{ki} (-A_{1i}A_{0i}) e_{-\tau} \right) d\tau + \\ \int_{-2\tau_d}^{-\tau_d} \left(e_{-\tau}^T \left(-A_{1i}^2\right)^T P_{ki} e(t) + e^T(t) P_{ki} \left(-A_{1i}^2\right) e_{-\tau} \right) d\tau + \\ \int_{-\tau_d}^{0} \gamma \left(p e^T P_{ki} e - e_{-\tau}^T P_{ki} e_{-\tau} \right) d\tau + \int_{-2\tau_d}^{-\tau_d} \gamma \left(p e^T P_{ki} e - e_{-\tau}^T P_{ki} e_{-\tau} \right) d\tau \end{array} \right) \tag{5c}$$

inequality of (5d) can be modified (by adding and subtracting terms $\int_{-\tau_d}^{0} e^T R_0 e d\tau$ and $\int_{-2\tau_d}^{-\tau_d} e^T R_1 e d\tau$) as (5e), shown at the bottom of the page. From (5e), it can be seen that the reaching criterion for orbital existence ($\dot{V}_k(e) < 0$) is satisfied if all of the matrix inequalities in (6a)–(6c), shown at the bottom of the page, are satisfied.

To combine the matrix inequalities in (6a)–(6c) and eliminate R_0 and R_1, the following theorem [26] is used:

Theorem 1: There exists a symmetric matrix X, such that

$$\begin{bmatrix} H_1 - LXL^T & U_1 \\ U_1^T & S_1 \end{bmatrix} > 0 \text{ and } \begin{bmatrix} H_2 + X & U_2 \\ U_2^T & S_2 \end{bmatrix} > 0$$

if and only if

$$\begin{bmatrix} H_1 + LH_2L^T & U_1 & LU_2 \\ U_1^T & S_1 & 0 \\ U_2^T L^T & 0 & S_2 \end{bmatrix} > 0.$$

Using Theorem 1, R_0 is first eliminated from inequalities (6a) and (6b). Next, R_1 is eliminated by applying Theorem 1 to the resultant LMI and (6c), and the following matrix inequality is obtained

$$\sum_{i=1}^{h} \alpha_{ki} \begin{bmatrix} G_{ki} & P_{ki}A_{1i}A_{0i} & -P_{ki}A_{1i}^2 & P_{ki}\bar{B}_i \\ -A_{0i}^T A_{1i}^T P_{ki} & -\gamma p P_{ki} & 0 & 0 \\ -\left(A_{1i}^2\right)^T P_{ki} & 0 & -\gamma P_{ki} & 0 \\ \bar{B}_i^T P_{ki} & 0 & 0 & 0 \end{bmatrix} < 0 \tag{7}$$

[1]Note that matrices R_0 and R_1 do not have any physical meaning and are introduced only to facilitate the derivation of (7) from (5c).

$$\dot{V}_k(e) < \sum_{i=1}^{h} \alpha_{ki} \left(\begin{array}{l} \begin{bmatrix} e \\ 1 \end{bmatrix}^T \begin{bmatrix} (A_{0i}+A_{1i})^T P_{ki} + P_{ki}(A_{0i}+A_{1i}) & \bar{B}_i^T P_{ki} \\ P_{ki}\bar{B}_i & 0 \end{bmatrix} \begin{bmatrix} e \\ 1 \end{bmatrix} + \\ \int_{-\tau_d}^{0} \begin{bmatrix} e^T & e_{-\tau}^T \end{bmatrix} \begin{bmatrix} \gamma p P_{ki} & P_{ki}(-A_{1i}A_{0i}) \\ (-A_{1i}A_{0i})^T P_{ki} & \gamma P_{ki} \end{bmatrix} \begin{bmatrix} e \\ e_{-\tau} \end{bmatrix} d\tau + \\ \int_{-2\tau_d}^{-\tau_d} \left(\begin{bmatrix} e^T & e_{-\tau}^T \end{bmatrix} \begin{bmatrix} \gamma p P_{ki} & P_{ki}\left(-A_{1i}^2\right) \\ \left(-A_{1i}^2\right)^T P_{ki} & \gamma P_{ki} \end{bmatrix} \begin{bmatrix} e \\ e_{-\tau} \end{bmatrix} \right) d\tau \end{array} \right) \tag{5d}$$

$$\begin{aligned} \dot{V}_k(e) &< \sum_{i=1}^{h} \alpha_{ki} \left(\begin{array}{l} \begin{bmatrix} e \\ 1 \end{bmatrix}^T \begin{bmatrix} (A_{0i}+A_{1i})^T P_{ki} + P_{ki}(A_{0i}+A_{1i}) & \bar{B}_i^T P_{ki} \\ P_{ki}\bar{B}_i & 0 \end{bmatrix} \begin{bmatrix} e \\ 1 \end{bmatrix} + \\ \int_{-\tau_d}^{0} \begin{bmatrix} e^T & e_{-\tau}^T \end{bmatrix} \begin{bmatrix} \gamma p P_{ki} & P_{ki}(-A_{1i}A_{0i}) \\ (-A_{1i}A_{0i})^T P_{ki} & \gamma P_{ki} \end{bmatrix} \begin{bmatrix} e \\ e_{-\tau} \end{bmatrix} d\tau + \\ \int_{-2\tau_d}^{-\tau_d} \left(\begin{bmatrix} e^T & e_{-\tau}^T \end{bmatrix} \begin{bmatrix} \gamma p P_{ki} & P_{ki}\left(-A_{1i}^2\right) \\ \left(-A_{1i}^2\right)^T P_{ki} & \gamma P_{ki} \end{bmatrix} \begin{bmatrix} e \\ e_{-\tau} \end{bmatrix} \right) d\tau + \\ \int_{-\tau_d}^{0} e^T R_0 e d\tau - \int_{-\tau_d}^{0} e^T R_0 e d\tau + \int_{-2\tau_d}^{-\tau_d} e^T R_1 e d\tau - \int_{-2\tau_d}^{-\tau_d} e^T R_1 e d\tau \end{array} \right) \\ &= \sum_{i=1}^{h} \alpha_{ki} \left(\begin{array}{l} \begin{bmatrix} e \\ 1 \end{bmatrix}^T \begin{bmatrix} (A_{0i}+A_{1i})^T P_{ki} + P_{ki}(A_{0i}+A_{1i}) + \tau_d(R_0+R_1) & P_{ki}\bar{B}_i \\ \bar{B}_i^T P_{ki} & 0 \end{bmatrix} \begin{bmatrix} e \\ 1 \end{bmatrix} \\ \quad + \int_{-\tau_d}^{0} \left(\begin{bmatrix} e^T & e_{-\tau}^T \end{bmatrix} \begin{bmatrix} \gamma p P_{ki} - R_0 & P_{ki}(-A_{1i}A_{0i}) \\ (-A_{1i}A_{0i})^T P_{ki} & \gamma P_{ki} \end{bmatrix} \begin{bmatrix} e \\ e_{-\tau} \end{bmatrix} \right) d\tau \\ \quad + \int_{-2\tau_d}^{-\tau_d} \left(\begin{bmatrix} e^T & e_{-\tau}^T \end{bmatrix} \begin{bmatrix} \gamma p P_{ki} - R_1 & P_{ki}\left(-A_{1i}^2\right) \\ \left(-A_{1i}^2\right)^T P_{ki} & \gamma P_{ki} \end{bmatrix} \begin{bmatrix} e \\ e_{-\tau} \end{bmatrix} \right) d\tau \end{array} \right) \end{aligned} \tag{5e}$$

$$\sum_{i=1}^{h} \alpha_{ki} \begin{bmatrix} (A_{0i}+A_{1i})^T P_{ki} + P_{ki}(A_{0i}+A_{1i}) + \tau_d(R_0+R_1) & P_{ki}\bar{B}_i \\ \bar{B}_i^T P_{ki} & 0 \end{bmatrix} < 0 \tag{6a}$$

$$\sum_{i=1}^{h} \alpha_{ki} \begin{bmatrix} \gamma p P_{ki} - R_0 & P_{ki}(-A_{1i}A_{0i}) \\ (-A_{1i}A_{0i})^T P_{ki} & \gamma P_{ki} \end{bmatrix} < 0 \tag{6b}$$

$$\sum_{i=1}^{h} \alpha_{ki} \begin{bmatrix} \gamma p P_{ki} - R_1 & P_{ki}\left(-A_{1i}^2\right) \\ \left(-A_{1i}^2\right)^T P_{ki} & \gamma P_{ki} \end{bmatrix} < 0. \tag{6c}$$

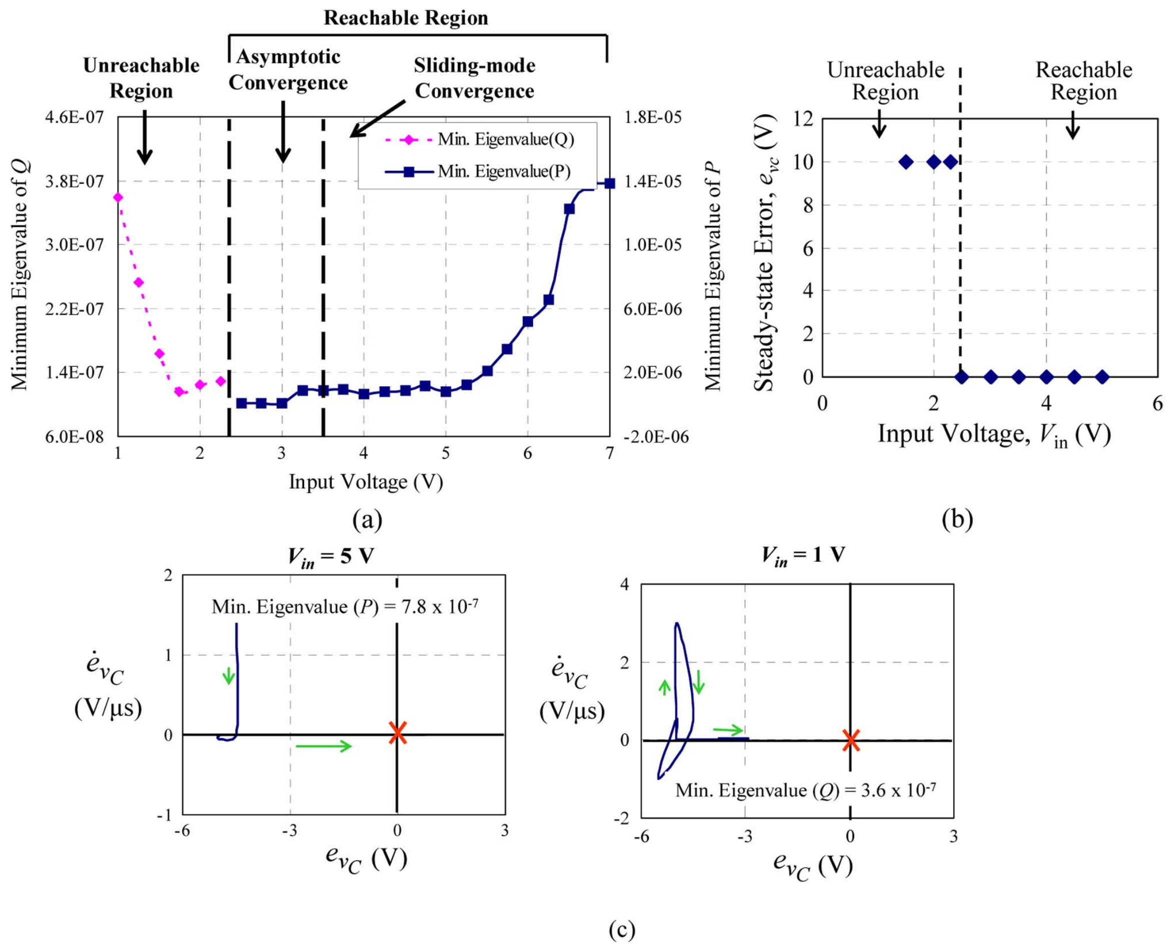

Fig. 9. (a) Variation of the minimum eigenvalues of the augmented P and Q matrices (obtained by solving LMIs (7), (12), and (10) for asymptotic convergence, sliding-mode convergence, and unreachable regions, respectively) with input voltage for an SPC operating in DCM with voltage-mode control. (b) Experimental results illustrating the reachable and unreachable regions with variation of the input voltage, V_{in}. (c) Experimental results illustrating state-error trajectories in the reachable ($V_{\mathrm{in}} = 5$ V) and unreachable ($V_{\mathrm{in}} = 1$ V) regions.

where $G_{ki} = (1)/(\tau_d)[(A_{0i} + A_{1i})^T P_{ki} + P_{ki}(A_{0i} + A_{1i})] + (\gamma p + \gamma)P_{ki}$. Because $0 \le \alpha_{ki} \le 1, \sum_{i=1}^{h} \alpha_{ki} = 1$, the matrix inequality in (7) can be represented as a conventional convex optimization problem [27] with LMI constraints. This convex optimization problem is of the class of *feasibility* problems, which involves obtaining a matrix P_{ki} such that the LMI in (7) is satisfied. These problems can be solved by using computationally efficient interior-point algorithms [28] and are available in common mathematical tools like MATLAB [29].

If there are no solutions of P_{ki} for (7) (which is automatically indicated in MATLAB when the total number of iterations exceed a default threshold), the dual of $V_k(e)$ is investigated to *confirm* that the error trajectories of the SPC states do not converge to the orbit [30], [31]. The dual of $V_k(e)$ is defined by

$$V_{Dk}(e) = \sum_{i=1}^{h} \lambda_{ki} e^T Q_{ki} e, \quad k = 1, 2, \ldots, M \tag{8}$$

where $0 \le \lambda_{ki} \le 1, \sum_{i=1}^{h} \lambda_{ki} = 1, Q_{ki} = Q_{ki}^T$ is a positive-definite matrix. To confirm that the state-error trajectories of the SPC do not converge to the orbit for the kth switching sequence, $V_{Dk}(e)$ has to satisfy the following criteria:

$$V_{Dk}(e) > 0 \text{ and } \dot{V}_{Dk}(e) > 0 \tag{9a}$$

$$\text{or } -V_{Dk}(e) = \sum_{i=1}^{h} \lambda_{ki} e^T(-Q_{ki})e < 0 \text{ and } -\dot{V}_{Dk}(e) < 0. \tag{9b}$$

As in (5)–(7), (9b) is satisfied, provided

$$\sum_{i=1}^{h} \lambda_{ki} \begin{bmatrix} T_{ki} & -Q_{ki}A_{1i}A_{0i} & Q_{ki}A_{1i}^2 & -Q_{ki}\bar{B}_i \\ A_{0i}^T A_{1i}^T Q_{ki} & \gamma p Q_{ki} & 0 & 0 \\ \left(A_{1i}^2\right)^T Q_{ki} & 0 & \gamma Q_{ki} & 0 \\ -\bar{B}_i^T Q_{ki} & 0 & 0 & 0 \end{bmatrix} < 0 \tag{10}$$

where

$$T_{ki} = -(1)/(\tau_d)[(A_{0i} + A_{1i})^T Q_{ki} + Q_{ki}(A_{0i} + A_{1i})] - (\gamma p + \gamma)Q_{ki}.$$

If there are no solutions of P_{ki} for (7) but, there exist solutions of Q_{ki} for (10), the state-error trajectories of the SPC do not converge to an orbit.

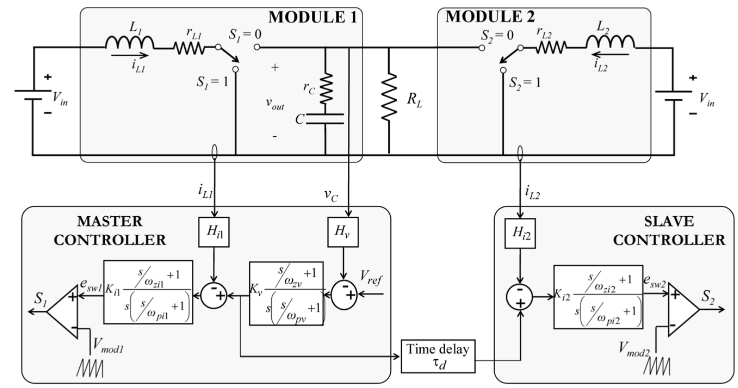

$$\dot{x} = A_{0i}x + A_{1i}x_{\tau_d} + B_i$$

$$x = \begin{bmatrix} i_{L1} \\ i_{L2} \\ v_C \\ \xi_1 \\ \xi_2 \\ \xi_3 \\ \xi_4 \\ \xi_5 \\ \xi_6 \end{bmatrix} \qquad A_{0i} = \begin{bmatrix} -\frac{1}{L_1}\left(r_{L1} + \frac{\bar{S}_1^2 R_L}{R_L + r_C}\right) & 0 & -\frac{1}{L_1}\frac{\bar{S}_1 R_L}{R_L + r_C} & 0 & 0 & 0 & 0 & 0 \\ 0 & -\frac{1}{L_2}\left(r_{L2} + \frac{\bar{S}_2^2 R_L}{R_L + r_C}\right) & -\frac{1}{L_2}\frac{\bar{S}_2 R_L}{R_L + r_C} & 0 & 0 & 0 & 0 & 0 \\ \frac{1}{C}\frac{\bar{S}_1 R_L}{R_L + r_C} & \frac{1}{C}\frac{\bar{S}_2 R_L}{R_L + r_C} & -\frac{1}{C}\frac{1}{R_L + r_C} & 0 & 0 & 0 & 0 & 0 \\ 0 & 0 & -1 & 0 & 0 & 0 & 0 & 0 \\ 0 & 0 & 0 & K_v & K_v\omega_{zv} & -\omega_{pi1} & 0 & 0 \\ -1 & 0 & 0 & 0 & 0 & 1 & 0 & 0 \\ 0 & -1 & 0 & 0 & 0 & 0 & -\omega_{pi2} & 0 \\ 0 & 0 & 0 & 0 & 0 & 0 & 1 & 0 \end{bmatrix}$$

$$B_i = \begin{bmatrix} \frac{V_{in}}{L_1} \\ \frac{V_{in}}{L_2} \\ 0 \\ V_{ref} \\ 0 \\ 0 \\ 0 \\ 0 \end{bmatrix} \qquad A_{1i} = \begin{bmatrix} 0 & 0 & 0 & 0 & 0 & 0 & 0 & 0 \\ 0 & 0 & 0 & 0 & 0 & 0 & 0 & 0 \\ 0 & 0 & 0 & 0 & 0 & 0 & 0 & 0 \\ 0 & 0 & 0 & 0 & 0 & 0 & 0 & 0 \\ 0 & 0 & 0 & 0 & 0 & 0 & 0 & 0 \\ 0 & 0 & 0 & 0 & 0 & 0 & 0 & 0 \\ 0 & 0 & 0 & K_v & K_v\omega_{zv} & 0 & 0 & 0 \\ 0 & 0 & 0 & 0 & 0 & 0 & 0 & 0 \end{bmatrix}$$

Switching conditions:

$$S_1 = \begin{cases} 0 & (K_{i1}\xi_3 + K_{i1}\omega_{z_{i1}}\xi_4) - V_{\mathrm{mod}\,1} \le 0 \\ 1 & (K_{i1}\xi_3 + K_{i1}\omega_{z_{i1}}\xi_4) - V_{\mathrm{mod}\,1} > 0 \end{cases}$$

$$S_2 = \begin{cases} 0 & (K_{i2}\xi_5 + K_{i2}\omega_{zi2}\xi_6) - V_{\mathrm{mod}\,2} < 0 \\ 1 & (K_{i2}\xi_5 + K_{i2}\omega_{zi2}\xi_6) - V_{\mathrm{mod}\,2} > 0 \end{cases}.$$

Fig. 10. Schematic and state-space equations of a two-module parallel boost SPC with master-slave architecture where current reference information is transmitted from the master module to the slave modules [33]. In the schematic, $V_{\rm in}$ represents the same input voltage source for both the modules.

B. Additional Reaching Criteria for Sliding-Mode and Mixed-Mode Convergences

If a SPC described by (1b) satisfies (7), it ensures the convergence of all the states of the SPC to their orbit. However, using this criterion, the different modes of convergences cannot be distinguished. Because certain modes of convergence (like sliding-mode convergence) typically have superior dynamics compared to others (like asymptotic-mode convergence), knowledge of the convergence mode can enable one to design a SPC with faster dynamic response. Thus, additional criteria are required to identify the mechanisms of convergences for the following cases.

Case A: N_1 Switching Surfaces are Orthogonal Sliding Surfaces: For a SPC with N switching surfaces ($e_{\rm sw1} = 0, \ldots, e_{{\rm sw}l} = 0, \ldots, e_{{\rm sw}N} = 0$), of which $N_1 (\le N)$ switching surfaces are orthogonal, the lth switching surface is a sliding surface provided that [17]–[20]

$$V_{lj}(e_{{\rm sw}l}) = e_{{\rm sw}l}^T P_{lj} e_{{\rm sw}l} > 0, \quad l = 1, 2, \ldots, N_1 \tag{11a}$$

$$\dot{V}_{lj}(e_{{\rm sw}l}) < 0 \tag{11b}$$

for all values of j where $j = 1, 2, \ldots, 2^{N_1}$ (for CCM) and $j = 1, 2, \ldots, 3^{N_1}$ (for DCM) represents the switching states on either side of the sliding surface, and $P_{lj} = P_{lj}^T$ are positive-definite matrices. By following a procedure similar to that in Section III.A, the lth switching surface is a sliding surface provided that the following j simultaneous LMIs are satisfied:

$$\begin{bmatrix} G_{lj} & P_{lj}A_{1j}A_{0j} & -P_{lj}A_{1j}^2 & P_{lj}\bar{B}_j \\ -A_{0j}^T A_{1j}^T P_{lj} & -\gamma p P_{lj} & 0 & 0 \\ -\left(A_{1j}^2\right)^T P_{lj} & 0 & -\gamma P_{lj} & 0 \\ \bar{B}_j^T P_{lj} & 0 & 0 & 0 \end{bmatrix} < 0 \tag{12}$$

where $G_{lj} = (1)/(\tau_d)[(A_{0j} + A_{1j})^T P_{lj} + P_{lj}(A_{0j} + A_{1j})] + (\gamma p + \gamma)P_{lj}$. For orthogonal sliding surfaces, convergence to the sliding manifold (defined by $e_{\rm sw1} = 0 \cap e_{\rm sw2} = 0 \cap \cdots \cap e_{{\rm sw}l} = 0 \cap \cdots \cap e_{{\rm sw}N_1} = 0$) is guaranteed if (12) is satisfied for all N_1 sliding surfaces.

Next, to investigate the convergence of the state-error trajectories from the sliding manifold to the orbit, a reduced-order

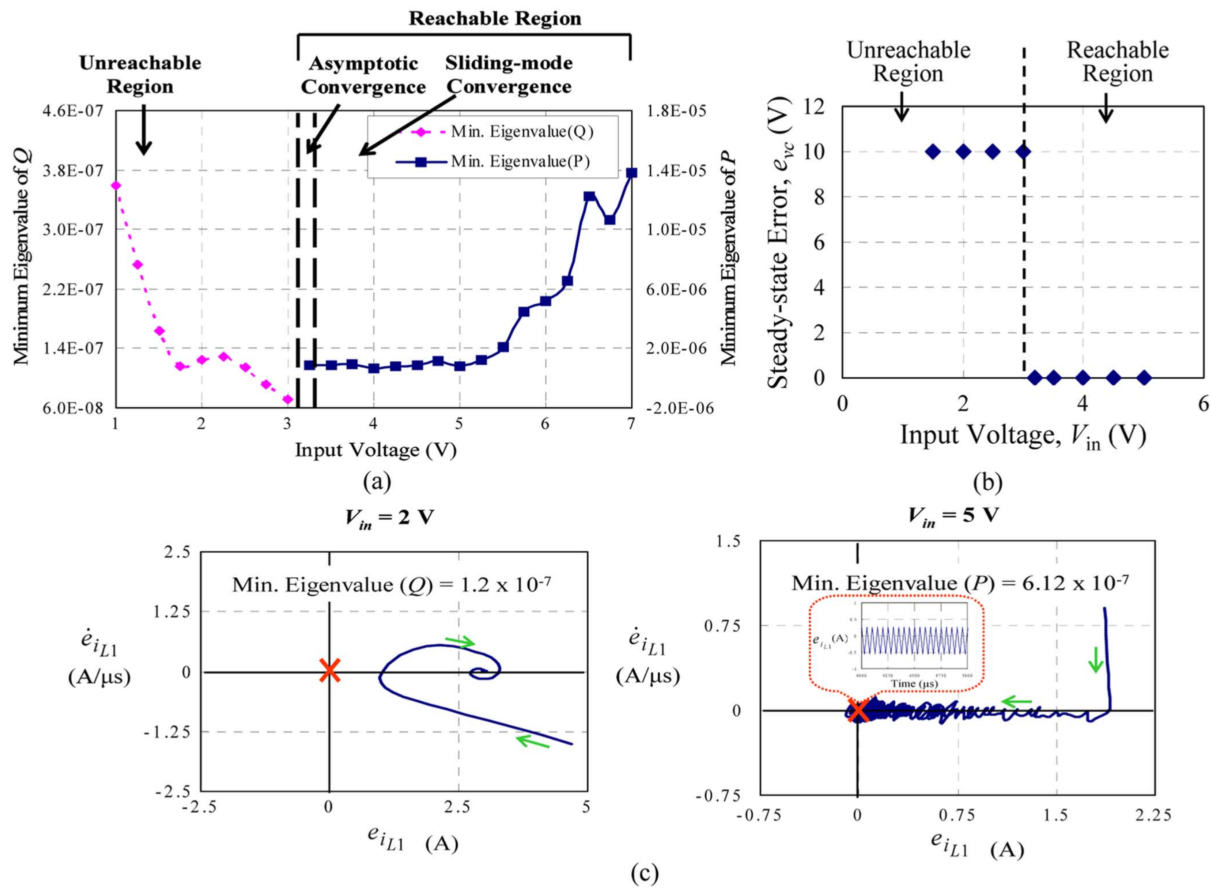

Fig. 11. (a) Variation of the minimum eigenvalues of the augmented P and Q matrices (obtained by solving LMIs (7) for asymptotic convergence, (12) and (17) for sliding-mode convergence, and (10) for unreachable regions, respectively) with input voltage for a two-module parallel dc–dc boost SPC with current-mode control scheme and interleaved PWM. (b) Experimental results illustrating the reachable and unreachable regions with variation of the input voltage, V_{in}. (c) Experimental results illustrating state-error trajectories in the reachable ($V_{\text{in}} = 5$ V) and unreachable ($V_{\text{in}} = 2$ V) regions. In (c), the error dynamics in the steady-state is also presented for the reachable case.

PWL model of the SPC in the error coordinates is developed. As in (2c), the model is given by

$$\dot{e}' = (A'_{0i} + A'_{1i})e' - \int_{-\tau_d}^{0} A'_{1i}A'_{0i}e'_{-\tau}d\tau - \int_{-2\tau_d}^{-\tau_d} A'^{2}_{1i}e'_{-\tau}d\tau + \bar{B}'_i \tag{13}$$

where $e' \in \Re^{(n-N_1)}$, and $A'_{0i}, A'_{1i} \in \Re^{(n-N_1)\times(n-N_1)}$. In (13), the order of the original SPC model is reduced by applying the sliding condition for the N_1 sliding surfaces, i.e., $e_{\text{sw}1} = 0, \ldots, e_{\text{sw}N_1} = 0$ [17]. To determine the reaching criteria for the reduced-order model, a procedure similar to that used for obtaining the general LMI (7) in Section II.A is followed. As in (3a) and (3b), the number of feasible combinations of switching sequences is

$$M_2 = \sum_{l=1}^{(2^{N_2}-W_2)} \left(\frac{(2^{N_2} - W_2)\,!}{l!\,(2^{N_2} - W_2 - l)\,!} \right)$$

$$M_2 = \sum_{l=1}^{(3^{N_2}-W_2)} \left(\frac{(3^{N_2} - W_2)\,!}{l!\,(3^{N_2} - W_2 - l)\,!} \right)$$

for the SPC operating in CCM and DCM, respectively. Here, $N_2 = N - N_1$ is the number of switching surfaces that do not exhibit sliding-mode convergence and W_2 is the number of redundant switching states of the reduced-order model. Following (4), a convex combination of multiple, positive-definite quadratic Lyapunov function is given by

$$V_k(e') = \sum_{i=1}^{h_2} \alpha_{ki} e'^T P'_{ki} e' > 0, \quad k = 1, 2, \ldots, M_2 \tag{14}$$

where h_2 is the number of switching states in a given sequence for the reduced-order model, $0 \le \alpha_{ki} \le 1, \sum_{i=1}^{h_2} \alpha_{ki} = 1$, and $P'_{ki} = P'^T_{ki}$ is a positive-definite matrix. As in (7), the reaching criterion is satisfied by the remaining states, provided

$$\sum_{i=1}^{h_2} \alpha_{ki} \begin{bmatrix} G'_{ki} & P'_{ki}A'_{1i}A'_{0i} & -P'_{ki}A'^2_{1i} & P'_{ki}\bar{B}'_i \\ -A'^T_{0i}A'^T_{1i}P'_{ki} & -\gamma' pP'_{ki} & 0 & 0 \\ -\left(A'^2_{1i}\right)^T P'_{ki} & 0 & -\gamma' P'_{ki} & 0 \\ \bar{B}'^T_i P'_{ki} & 0 & 0 & 0 \end{bmatrix} < 0 \tag{15}$$

where $G'_{ki} = (1)/(\tau_d)[(A'_{0i} + A'_{1i})^T P'_{ki} + P'_{ki}(A'_{0i} + A'_{1i})] + (\gamma' p + \gamma')P'_{ki}$ and $\gamma' > 0$ and $p' > 1$. Using (15), a criterion is developed to predict if the SPC state-error trajectories reach the orbit from the sliding manifold, described by $e_{\text{sw}1} = 0 \cap e_{\text{sw}2} = 0 \cap \cdots \cap e_{\text{sw}l} = 0 \cap \cdots \cap e_{\text{sw}N_1} = 0$.

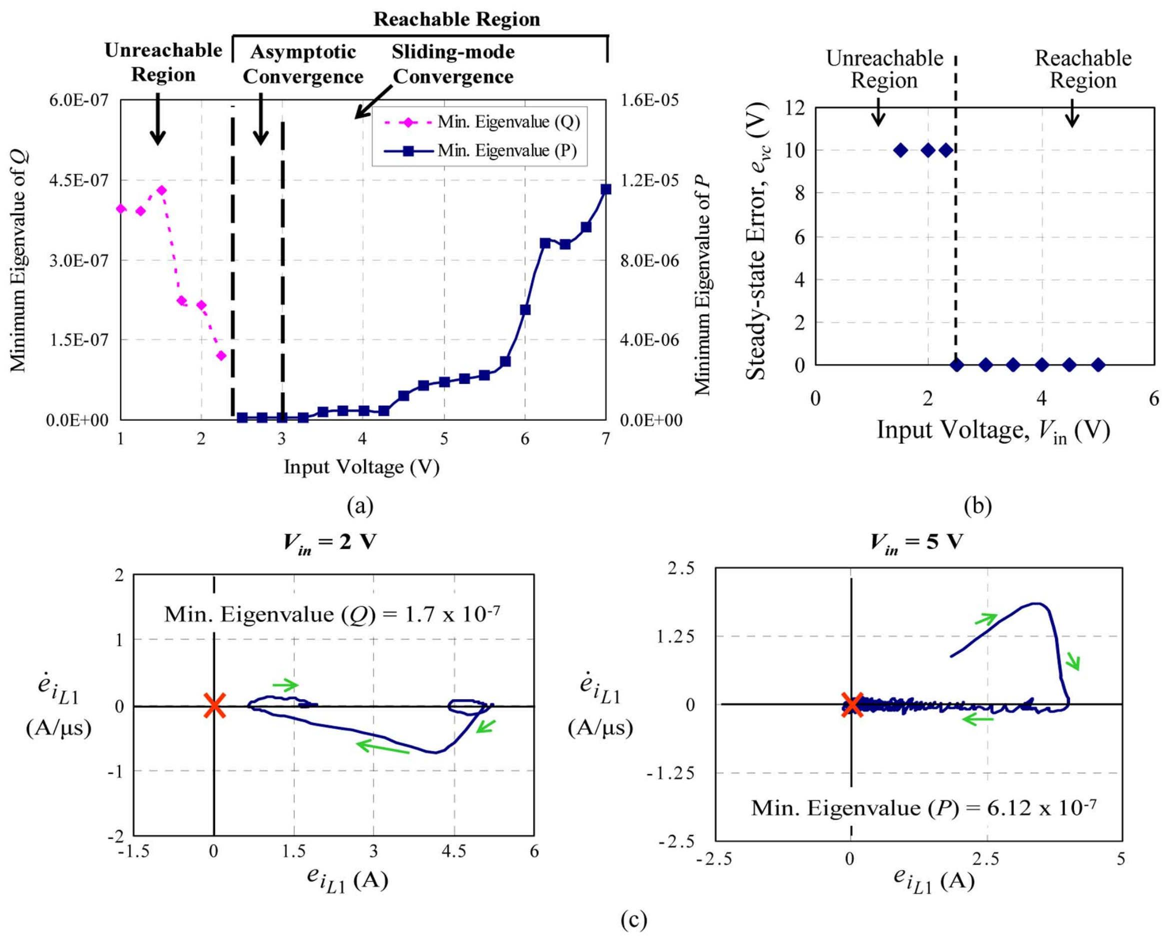

Fig. 12. (a) Variation of the minimum eigenvalues of the augmented P and Q matrices (obtained by solving LMIs (7) for asymptotic convergence, (12) and (17) for sliding-mode convergence, and (10) for unreachable regions, respectively) with input voltage for a two-module parallel dc–dc boost SPC with current-mode control scheme and synchronous PWM. (b) Experimental results illustrating the reachable and unreachable regions with variation of the input voltage, V_{in}. (c) Experimental results illustrating state-error trajectories in the reachable ($V_{\text{in}} = 5$ V) and unreachable ($V_{\text{in}} = 2$ V) regions.

TABLE II
PARAMETERS OF THE TWO-MODULE PARALLEL DC–DC BOOST SPC (FIG. 10)

POWER STAGE			CONTROLLER	
Parameter		**Nominal Values**	**Parameter**	**Nominal Values**
Switching frequency		100 kHz	Voltage controller gain, K_v	10000
Boost SPC output voltage		10 V	Voltage controller zero, ω_{zv}	100 rad/s
Peak output power		40 W	Voltage controller pole, ω_{pv}	20000 rad/s
Boost SPC input inductance	Module 2	128 μH	Current controller gain, K_{i1} and K_{i2}	15000
	Module 1	120 μH	Current controller zeros, ω_{zi1} and ω_{zi2}	1000 rad/s
Output capacitance		1000 μF	Current controller poles, ω_{pi1} and ω_{pi2}	25000 rad/s

Case B: N_1 Switching Surfaces are Sliding Surfaces But Not Orthogonal: For a SPC with N switching surfaces ($e_{\text{sw}1} = 0, \ldots, e_{\text{sw}l} = 0, \ldots, e_{\text{sw}N} = 0$), of which N_1 surfaces are sliding but not orthogonal to each other, a two-step procedure is employed. First, by following the procedure outlined in Case A, we determine whether each switching surface is sliding or not. If the switching surfaces satisfy (12), there exist N_1 nonorthogonal sliding switching surfaces, provided there exists a convex combination of multiple, positive-definite Lyapunov function, such that

$$V_k(e_{\text{sw}}) = \sum_{i=1}^{h_3} \alpha_{ki} e_{\text{sw}}^T P_{ki} e_{\text{sw}} > 0 \tag{16a}$$

$$\dot{V}_k(e_{\text{sw}}) < 0 \tag{16b}$$

where $e_{\text{sw}} = [e_{\text{sw}1} \ \cdots \ e_{\text{sw}N_1}]^T, h_3$ is the number of switching states in a given sequence, $0 \leq \alpha_{ki} \leq 1, \sum_{i=1}^{h_3} \alpha_{ki} =$

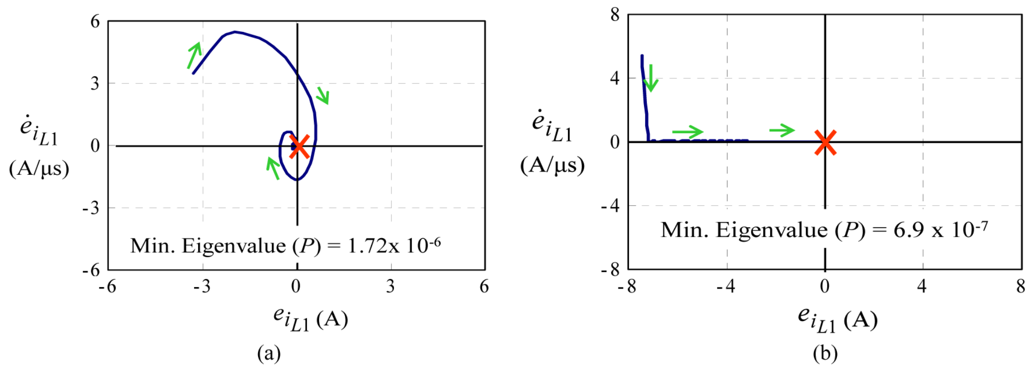

Fig. 13. Experimental results, illustrating state-error trajectories of a parallel dc–dc boost SPC, where (a) module 1 operates with carrier-based PWM and exhibits asymptotic convergence, and (b) module 2 operates with hysteretic modulation and exhibits sliding-mode convergence.

TABLE III
PARAMETERS OF THE CASCADED SPC CONSISTING OF A BOOST SPC FOLLOWED BY A BUCK SPC (FIG. 14)

POWER STAGE		CONTROLLER	
Parameter	**Nominal Values**	**Parameter**	**Nominal Values**
Switching frequency	100 kHz	Boost voltage controller gain, K_v	10000
Boost SPC output voltage	10 V	Boost voltage controller zero, ω_{zv}	100 rad/s
Peak output power	20 W	Boost voltage controller pole, ω_{pv}	20000 rad/s
Boost SPC input inductance	128 µH	Boost current controller gain, K_{i1}	15000
Boost SPC output capacitance	1000 µF	Boost current controller zero, ω_{zi1}	1000 rad/s
Buck output voltage	5 V	Boost current controller pole, ω_{pi1}	25000 rad/s
Buck SPC inductance	300 µH	Buck voltage controller gain, K_{v2}	10000
Buck SPC output capacitance	1000 µH	Buck voltage controller zero, ω_{zv2}	100 rad/s
		Buck voltage controller pole, ω_{pv2}	20000 rad/s
		Boost current controller gain, K_{i2}	15000
		Boost current controller zero, ω_{zi2}	1000 rad/s
		Boost current controller pole, ω_{pi2}	25000 rad/s

1, and $P_{ki} = P_{ki}^T$ is a positive-definite matrix. By following a procedure similar to the one derived earlier for the general case, all nonorthogonal switching surfaces are sliding, provided

$$\sum_{i=1}^{h_3} \alpha_{ki} \begin{bmatrix} G_{ki} & P_{ki}A_{1i}A_{0i} & -P_{ki}A_{1i}^2 & P_{ki}\bar{B}_i \\ -A_{0i}^T A_{1i}^T P_{ki} & -\gamma p P_{ki} & 0 & 0 \\ -\left(A_{1i}^2\right)^T P_{ki} & 0 & -\gamma P_{ki} & 0 \\ \bar{B}_i^T P_{ki} & 0 & 0 & 0 \end{bmatrix} < 0 \quad (17)$$

where $G_{ki} = (1)/(\tau_d)[(A_{0i} + A_{1i})^T P_{ki} + P_{ki}(A_{0i} + A_{1i})] + (\gamma p + \gamma)P_{ki}$. The condition to investigate whether the state-error trajectories approach the orbit from the sliding manifold, described by $e_{\mathrm{sw}1} = 0 \cap e_{\mathrm{sw}2} = 0 \cap \cdots \cap e_{\mathrm{sw}l} = 0 \cap \cdots \cap e_{\mathrm{sw}N_1} = 0$ can be determined by following the same procedure as in *Case A* and is given by (15).

IV. Results: Illustrations of Reaching-Criteria Applicability to Some Commonly Used SPCs

In this section, we first illustrate the application of the reaching criteria to a single-switch dc–dc boost SPC. Subsequently, we extend the reaching criteria to some higher order SPCs including 1) a two-module parallel connected dc–dc boost SPC; 2) a cascaded SPC consisting of a single-switch dc–dc boost SPC followed by a single-switch dc–dc buck SPC; and 3) a network of parallel connected three-phase VSIs. The goal of this paper is to demonstrate the applicability of the reaching criteria developed in this paper to different SPC topologies with varying control and modulation scheme. The proposed techniques can be used for further in-depth investigation of the impacts of different SPC parameters and control schemes on the reaching conditions for orbital existence and are part of our future research goals.

To illustrate the predictions of the proposed reaching criteria, the variations of the minimum eigenvalues of the augmented

$$P \left(= \begin{bmatrix} P_1 & 0 & 0 \\ 0 & \ddots & 0 \\ 0 & 0 & P_n \end{bmatrix} \right)$$

matrix for the reachable region and the augmented

$$Q \left(= \begin{bmatrix} Q_1 & 0 & 0 \\ 0 & \ddots & 0 \\ 0 & 0 & Q_n \end{bmatrix} \right)$$

TABLE IV
PARAMETERS OF THE THREE-PHASE VSI (FIG. 17)

POWER STAGE		CONTROLLER	
Parameter	**Nominal Values**	**Parameter**	**Nominal Values**
Input voltage, V_{in}	400 V	d-axis voltage loop gain, K_{d1}	20
Output line-line voltage	208 V (rms)	d-axis voltage loop zero, ω_{zd1}	10 rad/s
Power	2.5 kVA	d-axis voltage loop pole, ω_{pd1}	25000 rad/s
Switching frequency, f_{sw}	20 kHz	d-axis current controller gain, K_{rdi}	15000
Line inductors, L_r	1.5 mH	d-axis current controller zero, ω_{rzdi}	1000 rad/s
Output capacitances, C_r	10 μF	d-axis current controller pole, ω_{rpdi}	25000 rad/s
		q-axis current controller gain, K_{rqi}	10000
		q-axis current controller zero, ω_{rzqi}	100 rad/s
		q-axis current controller pole, ω_{rpqi}	20000 rad/s

matrix for the unreachable region are plotted, where $P_1 \cdots P_n$ and $Q_1 \cdots Q_n$ are obtained by solving the LMIs in (7), (10), (12), (15), and (17). Note that for positive-definite matrices, all of its eigenvalues are positive. Therefore, the minimum eigenvalue of P and Q can be used as to determine if the matrices obtained by solving the LMIs in (7), (10), (12), (15), and (17) are positive-definite or not.

The predictions of the theoretical analyses in Section III are validated with experimental results using the setups shown in Fig. 3 for the dc–dc SPCs and Fig. 18 for parallel connected three-phase VSIs. For both the cases, the controllers are implemented on a digital platform using TI DSP (TMS320C6713) and Altera FPGA (Flex10 K series). From a practical standpoint, to ensure that the components in the experimental setup do not exceed their rated currents and voltages, operating limits for the states of the power-stage are set. Therefore, in the experimental results presented in this paper, an orbit is considered to unreachable if the states of the power stage states reach the operation limits.

A. Single-Switch dc–dc Boost SPC

Fig. 4 shows the schematic and state-space equations of a single-switch dc–dc boost SPC following (1b). The parameters of the single-switch dc–dc boost SPC is given in Table I. Because the closed-loop system has no feedback delays $(\tau_d = 0), A_{1i} = 0$ in this case. When this SPC operates in CCM, the number of combinations of switching sequences, obtained using (3a) is three corresponding to either saturated operation with $S_1 = 0$ or $S_1 = 1$, or switching between $S_1 = 0$ and $S_1 = 1$ or vice versa.

1) Impacts of Parametric Variations: First, the impacts of variation in the input voltage on the reaching conditions of a single-switch dc–dc boost SPC with current-mode control, as illustrated in Fig. 4, are investigated. Fig. 5(a) illustrates the variation of the minimum eigenvalues of the augmented P and Q matrices with varying input voltage. The predictions of the reaching criteria are verified using experimental results, as shown in Fig. 5(b). The experimental results illustrated in Fig. 5(b) validate the prediction of the reaching criteria. Fig. 5(c) illustrates the phase portraits for two input voltages corresponding to the reachable and the unreachable regions, respectively. In these plots, the marker (x) indicates the desired equilibrium (corresponding to zero error at infinite frequency), while the arrows indicate how the state-error trajectories evolve with time. Additionally, the effects of load resistance (R_{L}), controller voltage-loop gain (K_{v}), and input inductance (L_1) on the reaching condition of the SPC are illustrated in Fig. 6. Using analyses similar to that illustrated in this paper, other parameters of the SPC can be varied as well to obtain the corresponding reachability bounds.

2) Effect of Control Schemes (Voltage-Mode- versus Current-Mode Control): In the previous section, the effects of variation of system parameters on the reaching conditions of a single-switch dc–dc boost SPC with current-mode control (based on full-state feedback) were investigated. Next , those results are compared with those obtained using a voltage-mode control scheme (based on partial feedback, where only the capacitor voltage is used for control). Fig. 7(a) illustrates how the reaching conditions of the SPC (with voltage-mode control) vary with input voltage. Comparison of these predictions with those in Fig. 5(a) indicates that the range of input voltages where the state-error trajectories converge to the orbit is smaller for the voltage-mode control scheme as compared to the current-mode control scheme. Using Figs. 5(b) and 7(b), we verify experimentally that for $\leq V_{\mathrm{in}} < 3$ V, the predictions of the reaching condition are satisfied for the current-mode control scheme but, not for the voltage-mode control scheme.

3) Impact of Modulation Strategies (Hysteresis versus Pulse-Width Modulation): Next, the reaching conditions for two different modulation schemes are investigated (with $V_{\mathrm{in}} = 2.75$ V); the first one is based on hysteretic modulation, where the switching condition is given by

$$S_1 = \begin{cases} 0, & e_{\mathrm{sw1}} \leq 0 \\ 1, & e_{\mathrm{sw1}} > 0 \end{cases} \tag{18}$$

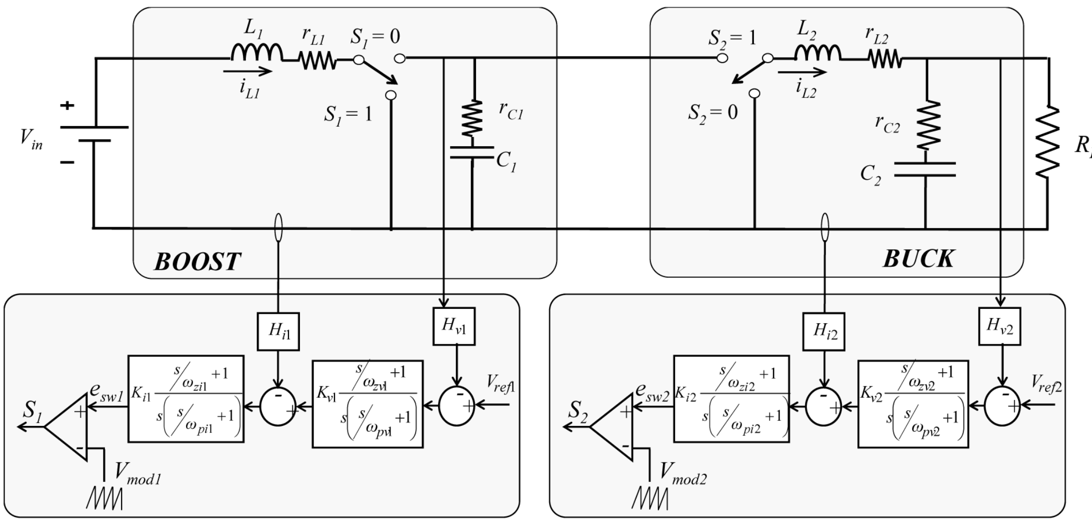

$$\dot{x} = A_{0i}x + A_{1i}x_{\tau_d} + B_i$$

$$A_{0i} = \begin{bmatrix}
-\frac{1}{L_1}\left(r_{L1}+r_{C1}\bar{S}_1\right) & -\frac{r_{L2}\bar{S}_2}{L_1} & -\frac{1}{L_1} & 0 & 0 & 0 & 0 & 0 & 0 & 0 & 0 & 0 \\
0 & \frac{\bar{S}_1}{C_1} & 0 & 0 & 0 & 0 & 0 & 0 & 0 & 0 & 0 & 0 \\
\frac{r_{L1}\bar{S}_1\bar{S}_2}{L_2} & -\frac{1}{L_2}\left(r_{C1}\bar{S}_2^2+\frac{r_{C2}R_L}{r_{C2}+R_L}-r_{L2}\right) & \frac{\bar{S}_2}{L_2} & 0 & 0 & 0 & 0 & 0 & 0 & 0 & 0 & 0 \\
0 & 0 & \frac{R_L}{C_2\left(r_{C2}+R_L\right)} & -\frac{1}{C_2\left(r_{C2}+R_L\right)} & 0 & 0 & 0 & 0 & 0 & 0 & 0 & 0 \\
0 & -1 & 0 & 0 & 0 & 0 & 0 & 0 & 0 & 0 & 0 & 0 \\
0 & 0 & 0 & 0 & 1 & 0 & 0 & 0 & 0 & 0 & 0 & 0 \\
-1 & 0 & 0 & 0 & K_{v1} & K_{v1}\omega_{zv1} & -\omega_{pi1} & 0 & 0 & 0 & 0 & 0 \\
0 & 0 & 0 & 0 & 0 & 0 & 1 & 0 & 0 & 0 & 0 & 0 \\
0 & 0 & 0 & -1 & 0 & 0 & 0 & 0 & 0 & 0 & 0 & 0 \\
0 & 0 & 0 & 0 & 0 & 0 & 0 & 1 & 0 & 0 & 0 & 0 \\
0 & 0 & -1 & 0 & 0 & 0 & 0 & 0 & K_{v2} & K_{v2}\omega_{zv2} & -\omega_{pi2} & 0 \\
0 & 0 & 0 & 0 & 0 & 0 & 0 & 0 & 0 & 0 & 1 & 0
\end{bmatrix}$$

$$x = \left[i_{L1} \; v_{C1} \; i_{L2} \; v_{C2} \; \xi_1 \; \xi_2 \; \xi_3 \; \xi_4 \; \xi_5 \; \xi_6 \; \xi_7 \; \xi_8\right]^T$$

$$B_i = \left[\frac{V_{in}}{L_1} \;\; 0 \;\; \frac{S_2 V_{in}}{L_2} \;\; 0 \;\; V_{ref\,1} \;\; 0 \;\; 0 \;\; V_{ref\,2} \;\; 0 \;\; 0 \;\; 0 \;\; 0\right]^T$$

Switching conditions:

$$S_1 = \begin{cases} 0 & \left(K_{i1}\xi_3 + K_{i1}\omega_{z_{i1}}\xi_4\right) - V_{mod\,1} \le 0 \\ 1 & \left(K_{i1}\xi_3 + K_{i1}\omega_{z_{i1}}\xi_4\right) - V_{mod\,1} > 0 \end{cases}; \qquad S_2 = \begin{cases} 0 & \left(K_{i2}\xi_7 + K_{i2}\omega_{zi2}\xi_8\right) - V_{mod\,2} < 0 \\ 1 & \left(K_{i2}\xi_7 + K_{i2}\omega_{zi2}\xi_8\right) - V_{mod\,2} > 0 \end{cases}.$$

Fig. 14. Schematic and state-space equations of a two-switch cascaded SPC, consisting of a front-end boost SPC followed by a buck SPC. For both the SPCs, current-mode control is used.

$e_{\mathrm{sw1}} = K_1(V_{\mathrm{ref}} - v_c(t)) + K_2 \int (V_{\mathrm{ref}} - v_c(t))dt$ and K_1 and K_2 are constant gains. For this case, the SPC exhibits sliding-mode convergence. For a ramp-based PWM scheme (shown in Fig. 4) with a voltage-mode controller, the error trajectories of the SPC converge asymptotically. The experimental results in Fig. 8 agree with the predictions of the reaching criteria developed in Section III.

4) Reaching Condition Under DCM: So far, we have discussed the reaching condition of a single-switch dc-dc boost SPC operating in CCM. Next, the reaching conditions of the same SPC operating in DCM are investigated. For DCM, the value of the input inductance (L_1) is chosen to be 15 μH. All other parameters are the same as for the case of CCM. The switching states are $S_1 = 0_C, S_1 = 0_D$, and $S_1 = 1$. Using (3b), the number of combinations of switching sequences for this SPC is 7. Fig. 9(a) shows how the reaching-condition bound of the SPC operating in DCM varies with change in input voltage. The experimental result in Fig. 9(b) and the state-error trajectories in Fig. 9(c) match the theoretical predictions. The predictions indicate that the range of reachable operating voltages for the SPC, operating in DCM, is larger than that of the SPC, operating in CCM.

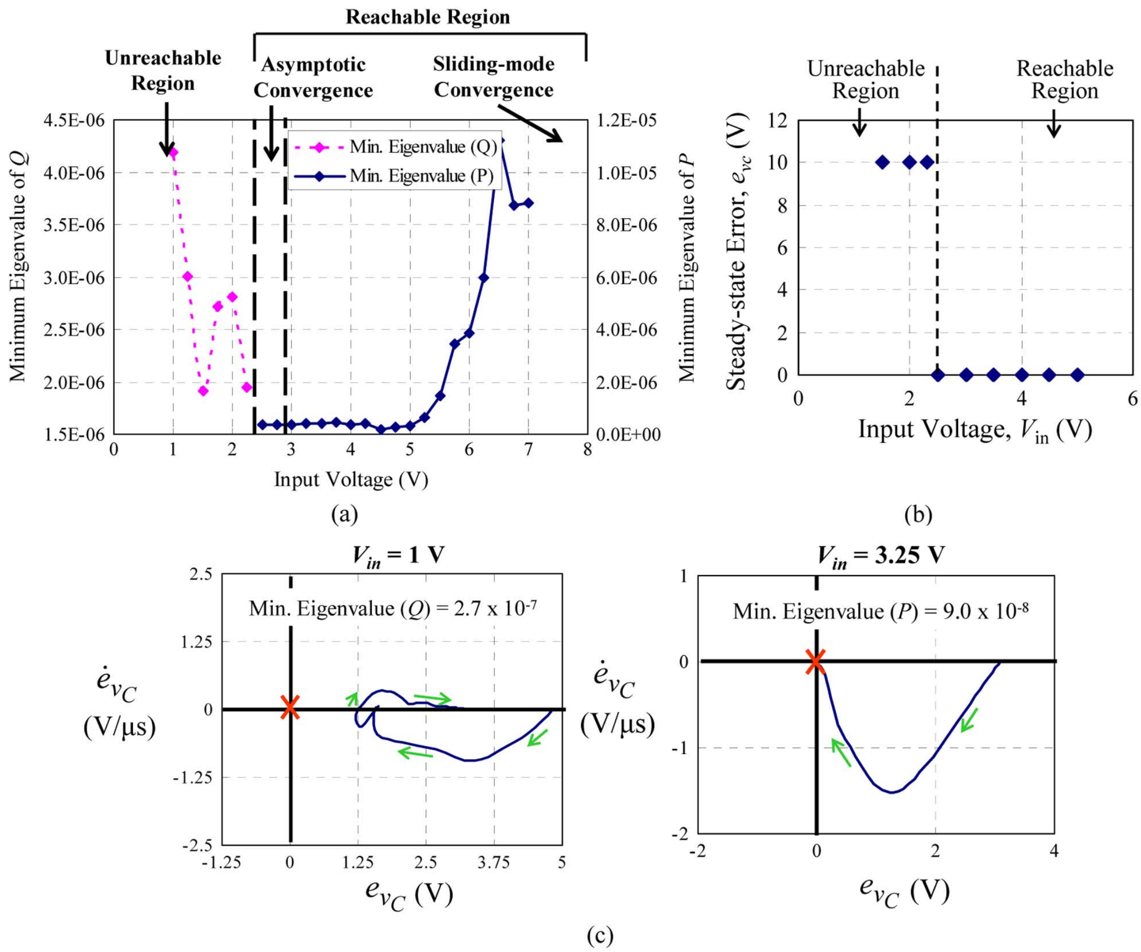

Fig. 15. (a) Variation of the minimum eigenvalues of the augmented P and Q matrices (obtained by solving LMIs (7), (12), and (10) for asymptotic convergence, sliding-mode convergence and unreachable regions, respectively) with input voltage. (b) Experimental results illustrating the reachable and unreachable regions with variation of the input voltage, $V_{\rm in}$. (c) Experimental results illustrating state-error trajectories for a cascaded SPC for $V_{\rm in} = 1$ V and $V_{\rm in} = 3.25$ V, where the boost SPC is turned on first with the buck SPC permanently turned on.

B. Extensions to Other Higher-Order Systems

In Section IV-A, theoretical predictions of the proposed reaching criteria for different parameters and operating conditions a single-switch dc–dc boost SPC were presented and these results were validated with experimental results. In this section, the extension of the proposed criteria to higher order SPCs is investigated.

1) Parallel dc–dc Boost SPC: Fig. 10 shows the schematic and state-space equations of a two-module parallel dc–dc boost SPC [32]. The parameters of this SPC are given in Table II. During the reaching period, the dynamics of this SPC differs from the single-switch dc–dc boost SPC because of differences in parameters of the different modules, phase shifts among modulating signals or time-delays in information transfer between the two modules [33]. For the two-module, parallel dc–dc SPC, the impact of phase shift in the PWM carrier signals of the converter modules on the reaching condition of the SPC is investigated. Two cases are considered, namely synchronous PWM, where the possible switching states are $S_1S_2 = 00$ and $S_1S_2 = 11$, and an interleaved PWM scheme, where the possible switching states are $S_1S_2 = 00, S_1S_2 = 01, S_1S_2 = 10,$ and $S_1S_2 = 11$. Figs. 11(a) and 12(a) illustrate how the reaching condition for such SPCs varies with input voltage. Both these schemes satisfy the reaching criteria for $V_{\rm in} > 3.25$ V. However, for $V_{\rm in} \leq 3.25$ V, the interleaved PWM scheme does not satisfy the reaching criteria. These predictions are confirmed by the experimental results presented in Figs. 11(b) and 12(b). Thus, while interleaved PWM schemes have inherent advantages like reduced output-voltage ripple, the range of input voltages in which it satisfies the reaching criteria is lower than the synchronous PWM based scheme.

Next, a scenario where the master module operates with a carrier-based PWM signal, while the slave module operates with hysteretic modulation is investigated (for $V_{\rm in} = 4$ V). From 13, we observe that the state-error trajectories of the slave and master modules exhibit sliding- and asymptotic-modes of convergences, respectively. While the LMI in (7) is satisfied for the entire SPC, the slave module also satisfies the sliding-mode convergence criterion in (12). The reduced-order model described in (13) satisfies the asymptotic convergence criteria (15).

2) Cascaded SPC Consisting of a Front-End Boost SPC Followed by a Buck SPC: Next, the reaching conditions for a two-switch cascaded SPC, consisting of a single-switch dc–dc boost

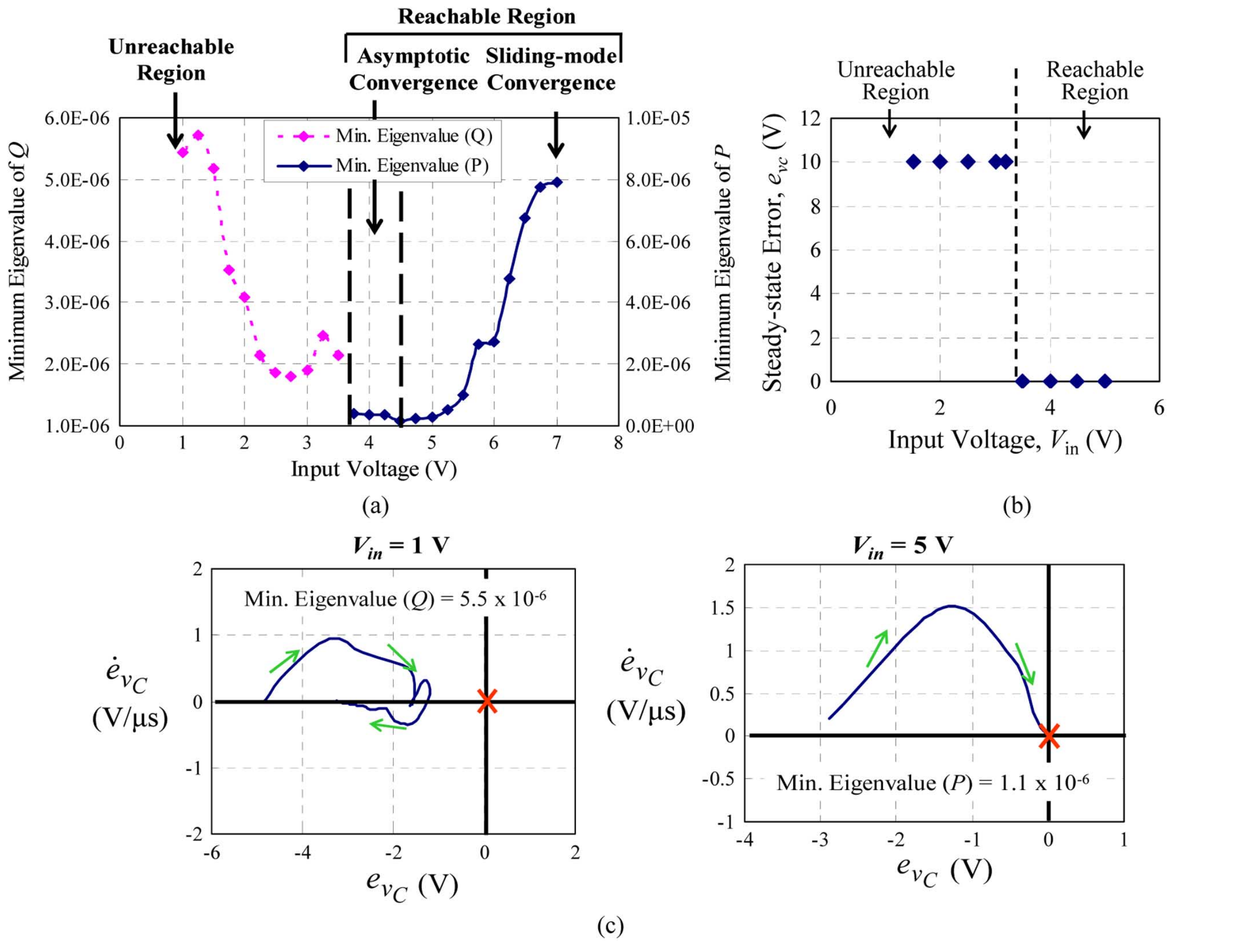

Fig. 16. (a) Variation of the minimum eigenvalues of the augmented P and Q matrices (obtained by solving LMIs (7), (12), and (10) for asymptotic convergence, sliding-mode convergence and unreachable regions, respectively). (b) Experimental results illustrating the reachable and unreachable regions with variation of the input voltage, V_{in}. (c) Experimental results illustrating state-error trajectories in the reachable ($V_{\text{in}} = 5$ V) and unreachable ($V_{\text{in}} = 1$ V) regions for a cascaded SPC, where both SPCs turned on at the same time.

SPC followed by a single-switch dc–dc buck SPC [34], as shown in Fig. 14 is investigated. The parameters of this SPC are given in Table III. For this SPC, the impacts of two start-up methodologies are compared: for the first case, we use the traditionally used methodology, where the boost SPC is first turned on, and allowed to reach its steady-state values, while the buck SPC is permanently turned off initially, and for the second case, both the SPCs are turned on at the same time. As a result, the following combinations of switching sequences are possible.

Case 1) When the buck SPC is turned off during start-up, the possible switching states are $S_1S_2 = 00$ and $S_1S_2 = 10$, when the boost SPC is saturated, or a combination of the two when the switches of the boost SPC switch within each time period. When the buck SPC is turned on, the possible switching sequences are $S_1S_2 = 00$ and $S_1S_2 = 10$ or $S_1S_2 = 01$ and $S_1S_2 = 11$, when the buck SPC operates in the saturated region, or a combination of $S_1S_2 = 00, S_1S_2 = 01, S_1S_2 = 10$, and $S_1S_2 = 11$.

Case 2) When both the SPCs start at the same time, all possible combinations of switching sequences can occur.

For the two cases outlined above, Figs. 15(a) and 16(a) show the predictions of the reaching condition with variations in the input voltage. For $V_{\text{in}} > 3.5$ V, the state-error trajectories of both Case 1 and Case 2 converge to the orbit. In Case 1, because the buck SPC is initially turned off, the overall system requires longer time to converge 13 to an orbit; therefore, for $V_{\text{in}} > 3.5$ V, the start-up mechanism of Case 2 is more beneficial from a dynamic response point of view. For $2.5 < V_{\text{in}} \leq 3.5$ V, the mechanism outlined in Case 1 should be used because the state-error trajectories corresponding to Case 2 do not converge for all possible combinations of switching sequences. These predictions are verified by the experimental results in Figs. 15(b) and 16(b).

3) Network of Parallel Connected Three-Phase VSIs: Finally, the case of an interconnected network of parallel-connected three-phase VSIs, as shown in Fig. 17 is considered. For deriving the reaching conditions of the system, the model of the parallel VSI is transformed to the dqz-reference frame using Park's transformation. Also, for the interconnected network, control information is exchanged over a wireless communication network [23]. For such SPCs, time-delay bounds, as shown in Fig. 19(a), can be obtained by varying the value of τ_d and obtaining $\tau_d = \tau_{d\max}$, where

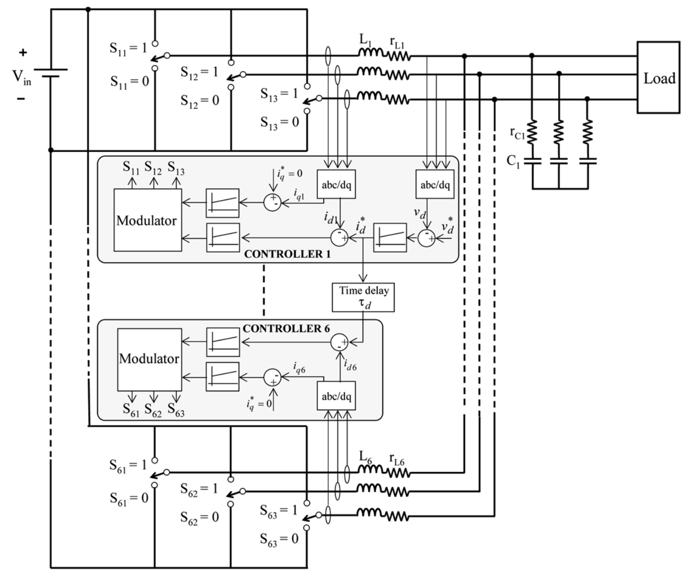

State-space equations of system: $\dot{x} = A_{0i}x + A_{1i}x_{\tau_d} + B_i$

$$x = \begin{bmatrix} x_{p\_1} \\ \vdots \\ x_{p\_6} \\ x_{c\_1} \\ \vdots \\ x_{c\_6} \end{bmatrix} \quad A_{0i} = \begin{bmatrix} A_{p\_10i} & \cdots & 0_{6\times6} & 0_{6\times6} & \cdots & 0_{6\times6} \\ \vdots & \ddots & \vdots & \vdots & \ddots & \vdots \\ 0_{6\times6} & \cdots & A_{p\_60i} & 0_{6\times6} & \cdots & 0_{6\times6} \\ H_1 & \cdots & 0_{6\times6} & A_{0c\_1} & \cdots & 0_{6\times6} \\ 0 & \ddots & \vdots & \vdots & \ddots & \vdots \\ 0_{6\times6} & \cdots & H_6 & 0_{6\times6} & \cdots & A_{0c\_6} \end{bmatrix}, \quad A_{1i} = \begin{bmatrix} 0_{6\times6} & \cdots & 0_{6\times6} & 0_{6\times6} & \cdots & 0_{6\times6} \\ \vdots & \ddots & \vdots & \vdots & \ddots & \vdots \\ 0_{6\times6} & \cdots & 0_{6\times6} & 0_{6\times6} & \cdots & 0_{6\times6} \\ 0_{6\times6} & \cdots & 0_{6\times6} & A_{1c\_1} & \cdots & 0_{6\times6} \\ 0 & \ddots & \vdots & \vdots & \ddots & \vdots \\ 0_{6\times6} & \cdots & 0_{6\times6} & 0_{6\times6} & \cdots & A_{1c\_6} \end{bmatrix}, \quad B_i = \begin{bmatrix} B_{p\_1i} \\ \vdots \\ B_{p\_6i} \\ B_{c\_1} \\ \vdots \\ B_{c\_6} \end{bmatrix}$$

H_r is a 6x6 matrix, whose non-zero elements are $H_{r\_14} = -\beta$, $H_{r\_31} = -1$, and $H_{r\_51} = -1$. The value of β for the master module is 1, while for the slave modules, its value is 0.

Power stage of each module: $\dot{x}_{p\_r} = A_{p\_r0i}x_{p\_r} + B_{p\_ri}$

$$x_{p\_r} = \begin{bmatrix} i_{Ldr} \\ i_{Lqr} \\ i_{Lzr} \\ \beta v_{Cd} \\ \beta v_{Cq} \\ \beta v_{Cz} \end{bmatrix} \quad A_{p\_r0i} = \begin{bmatrix} -\frac{1}{L_r}(r_{Lr}+r_C) & \omega & 0 & -\beta\frac{1}{L_r} & -\beta\frac{N_{inv}\omega r_C C}{L_r} & 0 \\ \omega & -\frac{1}{L_r}(r_{Lr}+r_C) & 0 & -\beta\frac{n\omega r_C C}{L_r} & -\beta\frac{1}{L_r} & 0 \\ 0 & 0 & -\frac{1}{L_r}(r_{Lr}+r_C) & 0 & 0 & -\beta\frac{1}{L_r} \\ -\beta\frac{1}{C} & 0 & 0 & \beta\frac{R}{R(R+r_C)} & -\beta N_{inv}\omega & 0 \\ 0 & -\beta\frac{1}{C} & 0 & -\beta N_{inv}\omega & 0 & 0 \\ 0 & 0 & -\beta\frac{1}{C} & 0 & 0 & 0 \end{bmatrix} \quad B_{p\_ri} = \begin{bmatrix} \frac{S_{dr}}{L_r}V_{in} \\ \frac{S_{qr}}{L_r}V_{in} \\ \frac{S_{zr}}{L_r}V_{in} \\ 0 \\ 0 \\ 0 \end{bmatrix}$$

where R is the load of the d-axis equivalent circuit, N_{inv} is the number of modules connected in parallel and ω is the frequency of the fundamental component of output voltage/current of the VSI.

Controller: $\dot{x}_{c\_r} = A_{0c\_r}x_{c\_r} + A_{1c\_r}x_{c\_r}(\tau_d) + B_{c\_r}$

$$x_{c\_r} = \begin{bmatrix} \beta\xi_1 \\ \beta\xi_2 \\ \xi_{r3} \\ \xi_{r4} \\ \xi_{r5} \\ \xi_{r6} \end{bmatrix} \quad A_{0c\_r} = \begin{bmatrix} -\beta\omega_{pd1} & 0 & 0 & 0 & 0 & 0 \\ \beta & 0 & 0 & 0 & 0 & 0 \\ \beta K_{d1} & \beta K_{d1}\omega_{zd1} & -\beta\omega_{pd1} & 0 & 0 & 0 \\ 0 & 0 & 1 & 0 & 0 & 0 \\ 0 & 0 & 0 & 0 & -\omega_{rpqi} & 0 \\ 0 & 0 & 0 & 0 & 1 & 0 \end{bmatrix} \quad B_{c\_r} = \begin{bmatrix} \beta V_{ref} \\ 0 \\ 0 \\ 0 \\ 0 \\ 0 \end{bmatrix}$$

$$A_{1c\_r} = \begin{bmatrix} 0 & 0 & 0 & 0 & 0 & 0 \\ 0 & 0 & 0 & 0 & 0 & 0 \\ \bar{\beta}K_{d1} & \bar{\beta}K_{d1}\omega_{zd1} & -\bar{\beta}\omega_{pd1} & 0 & 0 & 0 \\ 0 & 0 & 1 & 0 & 0 & 0 \\ 0 & 0 & 0 & 0 & -\omega_{rpqi} & 0 \\ 0 & 0 & 0 & 0 & 1 & 0 \end{bmatrix}, \quad \bar{\beta} = 1-\beta$$

Switching conditions:

$$S_{dr} = \begin{cases} 0 & (K_{rdi}\xi_{r3} + K_{rdi}\omega_{rzdi}\xi_{r4}) - V_{mod\ r1} \le 0 \\ 1 & (K_{rdi}\xi_{r3} + K_{rdi}\omega_{rzdi}\xi_{r4}) - V_{mod\ r1} > 0 \end{cases}, \quad S_{qr} = \begin{cases} 0 & (K_{rqi}\xi_{r5} + K_{rqi}\omega_{rzqi}\xi_{r6}) - V_{mod\ r2} \le 0 \\ 1 & (K_{rqi}\xi_{r5} + K_{rqi}\omega_{rzqi}\xi_{r6}) - V_{mod\ r2} > 0 \end{cases}.$$

Fig. 17. Schematic of a network of parallel connected three-phase VSIs and their state-space equations in the dqz-reference frame. For the results presented in this paper, r varies from 1–6.

the reaching criteria is not satisfied. The predictions are verified by the experimental results in Fig. 19(b). The data for the actual delay are obtained by using Markov-chain delay models, which are described in [23]. As the number of nodes increase, the time delay bounds decrease, while the actual time delay for information transfer increases. Such analyses can be used to estimate the maximum number of nodes that can be supported in the network.

V. Summary and Conclusion

A systematic analytical technique to analyze the reaching condition for orbital existence of a SPC is demonstrated. The multiple-Lyapunov-function based methodology outlined in this paper provides a mechanism for global stability analysis in conjunction with existing local stability analysis methodologies (e.g. those based on linearized averaged models, maps) by first establishing orbital existence and then ascertaining the stability of a periodic orbit. Currently, we are engaged in determining the stability of a periodic orbit using the multiple Lyapunov function approach. For a given periodic orbit, stability is established by transforming the problem of determining the matrix inequality (for orbital existence) to that of finding a matrix equality condition.

The orbital existence criteria outlined in this paper is derived based on nonrepetitive fundamental switching sequences based on non-redundant and complementary switching states of a SPC, which is described by a PWL model. The reaching criteria, being analytical, modulation independent and valid for all initial conditions for a given SPC and parametric set, needs significantly reduced computational overhead as compared to time-domain simulations. Apart from orbital existence, the reaching criteria can also predict various modes of convergences (including sliding- and asymptotic modes), which is beneficial for selecting parameters for enhanced dynamic performance. It can also be used for designing and analyzing hybrid control schemes [24].

In this paper, the practical application of the reaching criteria to a single and two-module dc-dc SPCs as well as a time-varying three-phase VSI is demonstrated. For the single-module dc-dc boost SPC, the effects of variations in the system parameters, control strategies, and operating conditions on the reaching condition bound is demonstrated. For two-module parallel and cascaded dc-dc SPCs, the impact of the two modulation schemes on the reaching condition is investigated. The results of the reaching criteria indicate that while interleaved PWM schemes have inherent advantages like reduced output-voltage ripple, the range of input voltage for which it satisfies the reaching criteria is lower than that obtained using the synchronous PWM based scheme. For a cascaded dc-dc SPC consisting of a front-end boost SPC followed by a dc-dc buck SPC, mechanisms to enhance dynamic performance during start-up are discussed. For a homogeneous network of parallel connected three-phase VSIs, the proposed analyses technique is used to determine the reachability bounds with variations of number of nodes and time delays. Such analyses can be used to estimate the maximum number of nodes that can be supported in a given network.

For large power networks, time delay in information transfer among the various SPCs is typically stochastic in nature. Therefore, techniques for reaching condition analyses proposed in this paper have to be re-formulated in a probabilistic framework [24]. In addition, as the size and complexity of the power network increases, the computational burden in determining the reachability bounds, using the proposed technique may increase. For such cases, development of techniques to simplify the reaching criteria has to be investigated. These are the foci of our ongoing research.

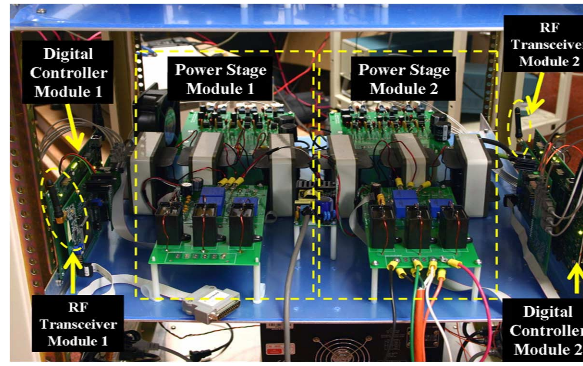

Fig. 18. Experimental setup for two modules of the network of parallel connected three-phase VSIs.

Appendix A
Definitions of Power Stage Matrices for Typical Single Switch DC-DC Converters

See Table V.

$$\dot{x}_p = A_{p\_i} x_p + b_{p\_i}, \quad S_1 = 0, 1$$

Appendix B
Illustration of Switching Sequences of a SPC With Two Switching Functions

In this section, an example is presented to show how the number of switching-sequence combinations (or M that is defined in Section III-A) is obtained. For a SPC with two switching functions (like the parallel dc–dc SPC in Fig. 10), the possible switching states are shown in Table VI. The combinations of switching sequences that are possible for such SPCs are shown in Table VII.

Thus, for a SPC with two switches, M is given by

$$M = {}^4C_1 + {}^4C_2 + {}^4C_3 + {}^4C_4 = 15. \tag{B1}$$

For certain SPCs, some switching states may be redundant. For instance, for a full-bridge dc–dc SPC with two switching functions, S_1 and S_2, the switching states $(S_1 = 0, S_2 = 0)$, and $(S_1 = 1, S_2 = 1)$ are redundant states and can be described by the same state-space equation. Thus, such redundant states have to be subtracted, while estimating the total number of combinations.

In general, for an SPC with N switching functions and W redundant switching states, the total number of combinations of l sequences is $(((2^N - W)!)/(l!(2^N - W - l)!))$. Also, for an SPC with N switching functions, $(2^N - W)$ possible set of

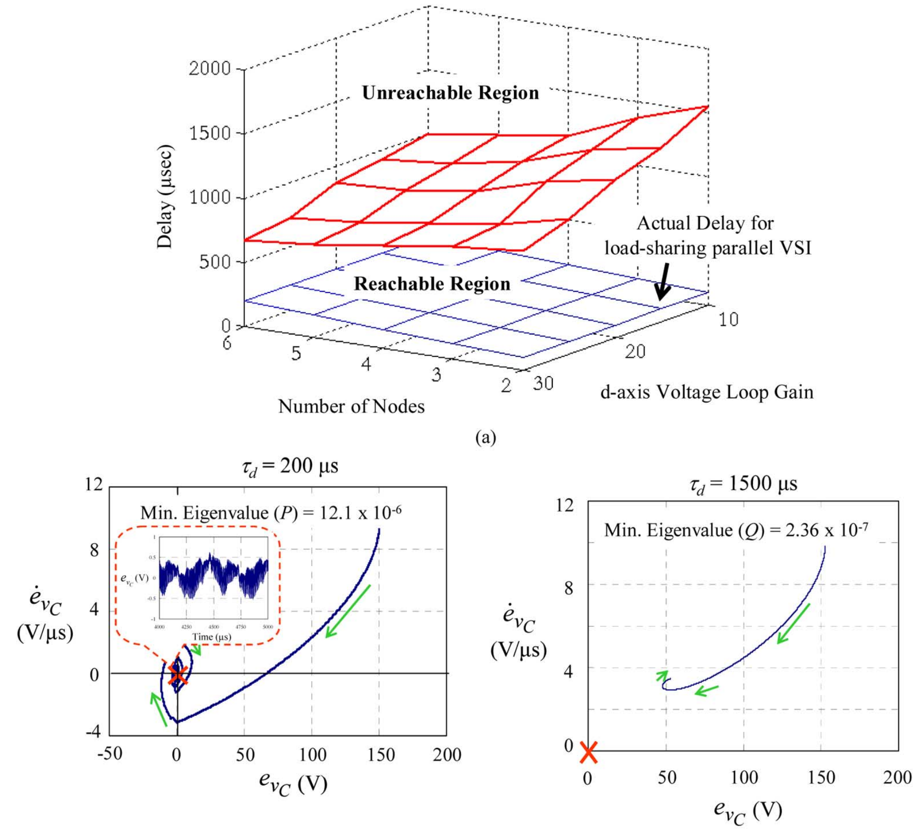

Fig. 19. (a) Reaching criterion prediction results (obtained by solving LMIs (7) and (10)) showing delay bounds for a network of parallel connected VSIs with voltage loop gain and the number of nodes. (b) Experimental results illustrating state-error trajectories in the reachable and unreachable regions. In (a), the bottom figure illustrates the error waveforms within the steady state. In (b), the error dynamics in the steady-state is also presented for the reachable case.

TABLE V
DEFINITIONS OF POWER STAGE MATRICES FOR TYPICAL SINGLE SWITCH DC-DC CONVERTERS

$$\dot{x}_p = A_{p\_i}x_p + b_{p\_i}, \qquad S_1 = 0{,}1$$

SPC TYPE	A_{p_i}	b_{p_i}	$x_p(t)$
Buck 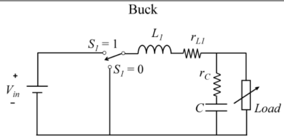	$\begin{bmatrix} -\frac{1}{L_1}\left(r_{L1}+\frac{r_C R}{R+r_C}\right) & -\frac{1}{L_1}\frac{R}{R+r_C} \\ \frac{R}{C(R+r_C)} & -\frac{1}{C(R+r_C)} \end{bmatrix}$	$\begin{bmatrix} \frac{S_1 V_{in}}{L_1} \\ 0 \end{bmatrix}$	$\begin{bmatrix} i_{L1} \\ v_C \end{bmatrix}$
Boost 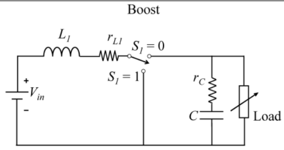	$\begin{bmatrix} -\frac{1}{L_1}\left(r_{L1}+\frac{(1-S_1)^2 R}{R+r_C}\right) & -\frac{1}{L_1}\frac{(1-S_1)R}{R+r_C} \\ \frac{1}{C}\frac{(1-S_1)R}{R+r_C} & -\frac{1}{C}\frac{1}{R+r_C} \end{bmatrix}$	$\begin{bmatrix} \frac{V_{in}}{L_1} \\ 0 \end{bmatrix}$	$\begin{bmatrix} i_{L1} \\ v_C \end{bmatrix}$
Buck-boost 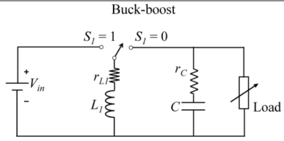	$\begin{bmatrix} -\frac{1}{L_1}\left(r_{L1}+\frac{(1-S_1)^2 R}{R+r_C}\right) & -\frac{(1-S_1)}{L_1}\left(\frac{r_C}{R+r_C}+1\right) \\ \frac{1}{C}\frac{(1-S_1)R}{R+r_C} & -\frac{1}{C}\frac{1}{R+r_C} \end{bmatrix}$	$\begin{bmatrix} \frac{S_1 V_{in}}{L_1} \\ 0 \end{bmatrix}$	$\begin{bmatrix} i_{L1} \\ v_C \end{bmatrix}$
Cuk' 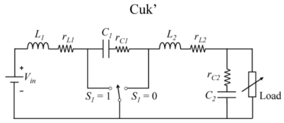	$\begin{bmatrix} -\frac{r_{L1}}{L_1} & -\frac{Z}{L_1}(r_{L2}+YRr_{C2}) & \frac{1}{L_1}(1+r_{C1}(1-S_1 Z)) & -\frac{R}{L_1 C_2}YZ \\ 0 & -\frac{Z}{L_2}(r_{L2}+YRr_{C2}) & \frac{S_1 Z}{L_2} & -\frac{RYZ}{L_2 C_2} \\ 0 & -\frac{Z}{C_1}(r_{L2}+YRr_{C2}) & \frac{S_2 Z}{C_1} & \frac{YZ}{C_1 C_2}R \\ 0 & \frac{RY}{C_2} & 0 & -\frac{Y}{C_2} \end{bmatrix}$ $Y=\frac{1}{R+r_{C2}}$ and $Z=\frac{1}{(1-Sr_{C1})}$	$\begin{bmatrix} \frac{V_{in}}{L_1} \\ 0 \\ 0 \\ 0 \end{bmatrix}$	$\begin{bmatrix} i_{L1} \\ i_{L2} \\ v_{C1} \\ v_{C2} \end{bmatrix}$

TABLE VI
POSSIBLE SWITCHING STATES FOR A SPC WITH TWO SWITCHING FUNCTIONS

i	S_1	S_2
1	0	0
2	0	1
3	1	0
4	1	1

sequences are possible. Thus, for a SPC with N switching functions and operating in CCM, M is given by

$$M = \sum_{l=1}^{(2^N-W)} \left({}^{(2^N-W)}C_l\right) = \sum_{l=1}^{(2^N-W)} \left(\frac{(2^N-W)!}{l!(2^N-W-l)!}\right). \tag{B2}$$

If the SPC operates in the DCM, the total number of switching states increase from $(2^N - W)$ to $(3^N - W)$, because each switching function has an additional state corresponding to $S = 0_D$, which represents DCM. For a SPC with N switching

TABLE VII
COMBINATIONS OF SWITCHING SEQUENCES THAT ARE POSSIBLE FOR SUCH SPCs

Number of States in a Sequence	***Switching Sequences***				***Total Number of Combinations***	***Illustration***
	First Switching State	***Second Switching State***	***Third Switching State***	***Fourth Switching State***		
1	$(i = 1)$				4	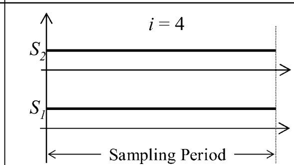
	$(i = 2)$					
	$(i = 3)$					
	$(i = 4)$					
2	$(i = 1)$	$(i = 2)$			6	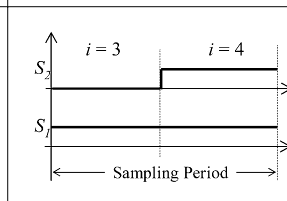
	$(i = 1)$	$(i = 3)$				
	$(i = 1)$	$(i = 4)$				
	$(i = 2)$	$(i = 3)$				
	$(i = 2)$	$(i = 4)$				
	$(i = 3)$	$(i = 4)$				
3	$(i = 1)$	$(i = 2)$	$(i = 3)$		4	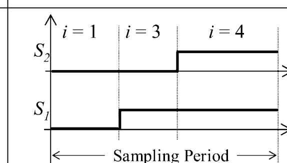
	$(i = 1)$	$(i = 2)$	$(i = 4)$			
	$(i = 1)$	$(i = 3)$	$(i = 4)$			
	$(i = 2)$	$(i = 3)$	$(i = 4)$			
4	$(i = 1)$	$(i = 3)$	$(i = 4)$	$(i = 2)$	1	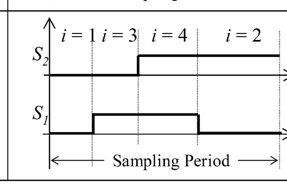

function and operating in DCM, the total number of feasible combinations is given by

$$M = \sum_{l=1}^{(3^N - W)} \left({}^{(3^N - W)}C_l \right) = \sum_{l=1}^{(3^N - W)} \left(\frac{(3^N - W)!}{l!(3^N - W - l)!} \right). \tag{B3}$$

ACKNOWLEDGMENT

The authors would like to thank Texas Instruments and Altera for their support in building the experimental setup for this work.

REFERENCES

[1] S. K. Mazumder and K. Acharya, "Multiple Lyapunov function based reaching condition analyses of switching power converters," in *Proc. IEEE Power Electron. Specialists Conf.*, Jun. 2006, pp. 2232–2239.

[2] R. D. Middlebrook and S. Cuk, "A general unified approach to modeling switching-converter power stages," in *Proc. IEEE Power Electron. Specialists Conf.*, 1977, pp. 521–550.

[3] F. C. Lee, *Modeling, Analysis, and Design of PWM Converter*, ser. Virginia Power Electronic Center Publications. Alta Loma, CA: SMPS Technology, 1990, vol. 2 [Online]. Available: http://www.smpstech.com/books/bookv.htm#VPEC0001

[4] S. K. Mazumder, A. H. Nayfeh, and D. Boroyevich, "Theoretical and experimental investigation of the fast- and slow-scale instabilities of a dc–dc converter," *IEEE Trans. Power Electron.*, vol. 16, no. 2, pp. 201–216, Mar. 2001.

[5] S. Banerjee and G. C. Verghese, Eds., *Nonlinear Phenomena in Power Electronics: Attractors, Bifurcations, Chaos, and Nonlinear Control*. Piscataway, NJ: IEEE Press, 2001.

[6] C. K. Tse, *Complex Behavior of Switching Power Converters*. Boca Raton, FL: CRC Press, 2004.

[7] C. Rivetta and G. A. Williamson, "Global behavior analysis of a dc–dc boost power converter operating with constant power load," in *Proc. IEEE Int. Symp. Circuits Syst.*, May 2004, vol. 5, pp. 956–959.

[8] X. Xu and G. Zhai, "New results on practical stabilization and practical reachability of switched systems," in *Proc. IEEE Amer. Contr. Conf.*, Jun. 2005, pp. 3784–3789.

[9] I. I. Mahmoud and S. A. Camels, "Using a simulation technique for switched mode high voltage power supplies performance study," *IEEE Trans. Ind. Appl.*, vol. 34, no. 5, pp. 945–952, Oct. 1998.

[10] M. Nakahara and T. Higashi, "A fast algorithm of steady-state and transient simulations for controlled switching power supplies," in *Proc. IEEE Int. Telecommun. Energy Conf.*, Nov. 1995, pp. 616–621.

[11] H. R. Visser and P. P. J. van den Bosch, "Modeling of periodically switching networks," in *Proc. IEEE Power Electron. Specialists Conf.*, Jun. 1991, pp. 67–73.

[12] R. Leyva, I. Queinnec, S. Tarbouriech, C. Alonso, and L. Martinez-Salamero, "Large-signal stability in high-order switching converter," in *Proc. IEEE Amer. Contr. Conf.*, Jun. 2004, pp. 59–64.

[13] D. Casadei, J. Clare, L. Empringham, G. Serra, A. Tani, A. Trentin, P. Wheeler, and L. Zarri, "Large-signal model for the stability analysis of matrix converters," *IEEE Trans. Ind. Electron.*, vol. 54, no. 2, pp. 939–950, Apr. 2007.

[14] P. C. Loh, D. M. Vilathgamuwa, C. J. Gajanayake, Y. R. Lim, and C. W. Teo, "Transient modeling and analysis of pulse-width modulated Z-source inverter," *IEEE Trans. Power Electron.*, vol. 22, no. 2, pp. 498–507, Mar. 2007.

[15] R. W. Erickson, S. Cuk, and R. D. Middlebrook, "Large-signal modeling and analysis of switching regulators," in *Proc. IEEE Power Electron. Specialists Conf.*, 1982, pp. 240–250.
[16] A. Nayfeh and B. Balachandran, *Applied Nonlinear Dynamics: Analytical, Computational, and Experimental Methods*. New York: Wiley, 1995.
[17] V. Utkin, *Sliding Modes in Control and Optimization*. New York: Springer-Verlag, 1992.
[18] A. F. Filippov, *Differential Equations With Discontinuous Right Hand Sides*. Norwood, MA: Kluwer, 1988.
[19] D. Milosavljevic, "General conditions for the existence of a quasi-sliding mode on the switching hyperplane in discrete variable structure systems," *J. Autom. Remote Contr.*, vol. 46, pp. 307–314, 1985.
[20] S. K. Mazumder, A. H. Nayfeh, and D. Boroyevich, "A new approach to the stability analysis of boost power-factor correction circuits," *J. Vibration Contr.*, vol. 9, pp. 775–789, 2003.
[21] M. Johansson, *Piecewise Linear Control Systems*. New York: Springer, 2002.
[22] S. Boyd, L. El-Ghaoui, E. Feron, and V. Balakrishnan, "Linear matrix inequalities in system and control theory," in *Society for Industrial and Applied Mathematics*. Philadelphia, PA: SIAM, 1994.
[23] K. Acharya, S. K. Mazumder, and M. Tahir, "Fault-tolerant wireless network control of load-sharing multiphase interactive power network," in *Proc. IEEE Power Electron. Specialists Conf.*, Jun. 2006, pp. 1167–1174.
[24] S. K. Mazumder and K. Acharya, "Global stability methodology for switching power converters," presented at the IEEE Power Electronics Specialists Conf., Tutorial Presentation., Orlando, FL, Jul. 2007.
[25] W. L. Brogan, *Modern Control Theory*. Upper Saddle River, NJ: Prentice Hall, 1990.
[26] K. Gu, V. L. Kharitonov, and J. Chen, *Stability of Time Delay Systems*. Boston, MA: Birkhauser, 2003.
[27] S. Boyd and L. Vandenberghe, *Convex Optimization*. New York: Cambridge Univ. Press, 2004.
[28] Y. Nesterov and A. Nemirovskii, "An interior-point method for generalized linear-fractional problems," *J. Mathem. Programm.: Series B*, vol. 69, no. 1, pp. 177–204, Jul. 1995.
[29] P. Gahinet, A. Nemirovskii, A. J. Laub, and M. Chilali, "The LMI control toolbox," in *Proc. IEEE Con. Decision Contr.*, Lake Buena Vista, FL, Dec. 1994, vol. 3, pp. 2038–2041.
[30] G. Feng, "Stability analysis of piecewise discrete-time linear systems," *IEEE Trans. Autom. Contr.*, vol. 4, no. 7, pp. 1108–1112, Jul. 2002.
[31] R. Goebel, T. Hu, and A. R. Teel, "Dual matrix inequalities in stability and performance analysis of linear differential/difference inclusions," in *Current Trends in Nonlinear Systems and Control*. Boston, MA: Birkhauser, 2005.
[32] V. J. Tottuvelil and G. C. Verghese, "Analysis and control design of paralleled dc/dc converters with current sharing," *IEEE Trans. Power Electron.*, vol. 13, no. 4, pp. 635–644, Jul. 1998.
[33] S. K. Mazumder, M. Tahir, and K. Acharya, "Master-slave current-sharing control of a parallel dc–dc converter system over an RF communication interface," *IEEE Trans. Ind. Electron.*, vol. 55, no. 1, pp. 59–66, Jan. 2008.
[34] J. A. Morales-Saldana, E. E. C. Gutierrez, and J. Levya-Ranos, "Modeling of switch-mode dc–dc cascade converters," *IEEE Trans. Aerosp. Electron. Syst.*, vol. 38, no. 1, pp. 295–299, Jan. 2002.

Sudip K. Mazumder (SM'02) is the Director of Laboratory for Energy and Switching-electronics Systems (LESES) and an Associate Professor in the Department of Electrical and Computer Engineering at the University of Illinois, Chicago.

He has over 12 years of professional experience and has held R&D and design positions in leading industrial organizations. His current areas of interests are interactive power-electronics/power networks, renewable and alternate energy systems, photonically triggered power semiconductor devices, and systems-on-chip/module (i.e., SoC/SoM). He has published over 60 refereed and invited journal and conference papers and is a reviewer for six international journals.

Dr. Mazumder received the prestigious 2008 Faculty Research Award and the 2006 Diamond Award from the University of Illinois, Chicago for Outstanding Research performance. He also received the ONR Young Investigator Award, NSF CAREER, and the DOE SECA awards in 2005, 2003, and 2002, respectively, and the Prize Paper Award from the IEEE TRANSACTIONS ON POWER ELECTRONICS and the IEEE PELS in 2002. He is the Editor-in-Chief for *International Journal of Power Management Electronics* since 2006. He is also an Associate Editor for the IEEE TRANSACTIONS ON INDUSTRIAL ELECTRONICS since 2003 and was the Associate Editor for IEEE POWER ELECTRONICS LETTERS until 2005. He has been invited by both IEEE and ASME for several keynote and plenary lectures. He presented a tutorial titled "Global stability methodologies for switching power converters" at the IEEE Power Electronics Specialists Conference, 2007. He also co-received the 2007 IEEE Outstanding Student Paper Award at the IEEE International Conference on Advanced Information Networking and Applications with his Ph.D. student M. Tahir.

Kaustuva Acharya (S'07) received the B.Eng. degree in electronics and communication engineering from the Regional Engineering College (now, the National Institute of Technology), Bhopal, India, in 2000, and the M.Sc. degree in electrical engineering from the University of Illinois, Chicago, in 2003, where he is currently pursuing the Ph.D. degree in electrical engineering.

He is a Research Assistant at the Laboratory for Energy and Switching-Electronics Systems, University of Illinois at Chicago. His research interests include power electronics for renewable and alternate energy sources, and modeling, analyses, and control of interactive power networks for distributed power systems. He has published over 15 refereed international journal and conference papers .

Mr. Acharya is a reviewer for IEEE TRANSACTIONS OF POWER ELECTRONICS and IEEE TRANSACTIONS ON INDUSTRIAL ELECTRONICS and several international conferences. He co-presented a tutorial titled "Global stability methodologies for switching power converters" at the IEEE Power Electronics Specialists Conference, 2007.